

A third-generation wave model for coastal regions

1. Model description and validation

N. Booij, R. C. Ris,¹ and L. H. Holthuijsen

Faculty of Civil Engineering, Delft University of Technology, Delft, Netherlands

Abstract. A third-generation numerical wave model to compute random, short-crested waves in coastal regions with shallow water and ambient currents (Simulating Waves Nearshore (SWAN)) has been developed, implemented, and validated. The model is based on a Eulerian formulation of the discrete spectral balance of action density that accounts for refractive propagation over arbitrary bathymetry and current fields. It is driven by boundary conditions and local winds. As in other third-generation wave models, the processes of wind generation, whitecapping, quadruplet wave-wave interactions, and bottom dissipation are represented explicitly. In SWAN, triad wave-wave interactions and depth-induced wave breaking are added. In contrast to other third-generation wave models, the numerical propagation scheme is implicit, which implies that the computations are more economic in shallow water. The model results agree well with analytical solutions, laboratory observations, and (generalized) field observations.

1. Introduction

Waves at the surface of the deep ocean can be well predicted with third-generation wave models that are driven by predicted wind fields [e.g., *WAMDI Group*, 1988; *Komen et al.*, 1994]. These are all based on the energy or action balance equation, sometimes extended to shelf seas by adding the finite-depth effects of shoaling, refraction and bottom friction [e.g., *Tolman*, 1991]. These models cannot be realistically applied to coastal regions with horizontal scales less than 20–30 km and water depth less than 20–30 m (with estuaries, tidal inlets, barrier islands, tidal flats, channels, etc.), because (1) the shallow-water effects of depth-induced wave breaking and triad wave-wave interaction are not included and (2) the numerical techniques that are used are prohibitively expensive when applied to such small-scale, shallow-water regions. It is the purpose of the present study to develop an effective and efficient wave model for these regions based on state-of-the-art formulations.

Two alternatives seem to be available: (1) extend the above (phase averaged) approach of the energy or action balance equation by adding the required physical processes using other numerical techniques or (2) exploit the alternative approach of phase-resolving models based on mass and momentum balance equations. Such phase-resolving models are usually based on Hamiltonian equations [e.g., *Miles*, 1981; *Radder*, 1992], Boussinesq equations [e.g., *Peregrine*, 1966; *Freilich and Guza*, 1984; *Madsen and Sørensen*, 1992], or on the mild-slope equation (e.g., *Berkhoff* [1972] or its parabolic version, e.g., *Radder* [1979] and *Kirby* [1986]). For a recent review, see *Dingemans* [1997]. These models reconstruct the sea surface elevation in space and time while accounting for such effects as refraction, diffraction, and, in some models, also triad and quadruplet wave-wave interactions. Dissipation processes such as bottom

friction and depth-induced wave breaking can be added, but wave generation by wind is absent in these models, which is unacceptable for many applications in coastal regions where storm conditions are often of particular interest (e.g., wave generation behind shoals or barrier islands). Moreover, the space and time resolutions that are required for these models are of the order of a small fraction of the wave length and period. This limits the practical application of these models to regions with dimensions that are smaller than about a dozen wavelengths ($1 \text{ km} \times 1 \text{ km}$, say).

For applications on a larger scale, phase-averaged models need to be used. These are either of a Lagrangian nature or of a Eulerian nature. In Lagrangian models the waves are propagated from deep water to the shore by transporting the wave energy along wave rays [*Collins*, 1972; *Cavaleri and Malanotte-Rizzoli*, 1981]. Adding the effects of wave generation and dissipation is possible, but these Lagrangian models are numerically inefficient when nonlinear effects such as wave breaking or wave-wave interactions are to be accounted for. It is more efficient to use the Eulerian approach, in which the wave evolution is formulated on a grid. This is essentially the technique that has been used for deep-ocean or shelf-sea wave models such as the Wave Model (WAM) [*WAMDI Group*, 1988]. All relevant processes are then readily included as sources and sinks in the basic equation. Drawbacks of this approach in coastal waters are the absence of diffraction and the use of linear wave theory for wave propagation. The first drawback implies that the area of interest should be a few wave lengths away from obstacles with (near)vertical walls (depending on the short-crestedness of the waves [*Booij et al.*, 1992]). This is often the case along fairly open coasts with an occasional small island or breakwater in the far field, as opposed to confined situations such as in a harbor or directly behind breakwaters. The second drawback implies that, for the model to be applicable, nonlinear corrections to linear wave propagation should either be sufficiently well represented by triad and quadruplet wave-wave interactions or that they be dominated by the generation or dissipation of the waves (these processes can all be included in a phase-averaged model). The latter is often the case, even in the absence of wind, when waves break in shallow

¹Now at WL/Delft Hydraulics, Delft, Netherlands.

water. Since these limitations seem to be acceptable in many real field situations on a scale of 20–30 km with a water depth less than 20–30 m, the model to be developed in the present study is a phase-averaged, Eulerian model (see *Battjes* [1994] for a review of similar considerations).

Eulerian, phase-averaged models have been used for waves in the deep ocean and in water of intermediate depth since the pioneering work of *Gelci et al.* [1956], and extensive work has been done with these models [e.g., *Cardone et al.*, 1976; *WAMDI Group*, 1988; *Komen et al.*, 1994]. The propagation of waves in these models is readily extended to finite-depth water by introducing a depth-dependent propagation speed and a Eulerian representation of refraction [*Piess*, 1965; *Hasselmann et al.*, 1973]. However, these models do not compute all relevant physical processes for finite-depth water, in particular, not depth-induced wave breaking and triad wave-wave interactions, which, for coastal regions, can be rather important. Moreover, all these models are based on explicit numerical schemes for propagation which are subject to the Courant criterion for numerical stability. For oceanic conditions this is not a problem, but for coastal applications it is unacceptable, as it leads to very small time steps in the computations (the spatial step in ocean models is of the order of 100 km, and the corresponding time step is typically 30 min; in coastal models, in 10-m water depth, the numbers are typically 100 m and 10 s, respectively). The situation is aggravated by the fact that coastal models typically contain 2–5 times as many geographic grid points as ocean models. The application of explicit schemes in coastal situations would therefore require about 2 orders of magnitude more computational effort than in deep water. The solution to this problem is to use implicit numerical schemes which are unconditionally stable and therefore not subject to the Courant criterion. These two problems, of adding depth-induced breaking and triad wave-wave interactions and of using implicit numerical schemes, will be addressed in detail for the development of the model of the present study (Simulating Waves Nearshore (SWAN)).

State-of-the-art formulations of the processes of wave generation, dissipation, and wave-wave interactions in phase-averaged models are presently third generation. In first-generation models these physical processes are not properly represented. Generation is simulated with simple empirical expressions, and dissipation (whitecapping) is simulated with an assumed universal upper limit of the spectral densities. The absence of quadruplet wave-wave interactions is compensated by enhancing the wave growth [e.g., *Ewing*, 1971]. Second-generation models try to remedy this for the local wind sea by parameterizing these interactions [e.g., *Young*, 1988] or by using a sea-state- and wind-dependent upper limit of the spectral densities [e.g., *Holthuijsen and De Boer*, 1988] or by reducing the wave description to a few integral spectral parameters [e.g., *Hasselmann et al.*, 1976]. Such models are usually supplemented with freely propagating swell. In a third-generation model all relevant processes are represented explicitly without a priori restrictions on the evolution of the spectrum. For the development of these models, *Hasselmann et al.* [1985] formulated the discrete interaction approximation (DIA) of the quadruplet wave-wave interactions. This first-principle approach of the quadruplet wave-wave interactions permits the generation of waves by wind to be formulated on the basis of theoretical work of *Miles* [1957] and the empirical work of *Snyder et al.* [1981]. For deep water the problem was finally closed with the formulation of whitecapping by *Komen et al.* [1984]. The

prototypical third-generation model that was developed on the basis of these formulations is the WAM model of the *WAMDI Group* [1988] (also see *Komen et al.* [1994]). Other third-generation models are the WAVEWATCH model of *Tolman* [1991], the model of *Li and Mao* [1992], the Program for Hindcasting of Waves in Deep, Intermediate and Shallow Water (PHIDIAS) model of *Van Vledder et al.* [1994], and the Telemac Based Operational Model Addressing Wave Action Computation (TOMAWAC) model of *Benoit et al.* [1996]. For shallow water the formulations for the deepwater processes need to be adapted and extended. This has been achieved, to some extent, in the above third-generation models with (1) the use of the shallow-water phase speed in the expressions of wind input, (2) a depth-dependent scaling of the quadruplet wave-wave interactions, (3) a reformulation of the whitecapping in terms of wave number rather than frequency, and (4) adding bottom dissipation. All this will be also used in the SWAN model and supplemented with formulations for (5) depth-induced wave breaking and (6) triad wave-wave interactions that have been developed specifically for SWAN (and similar models) by *Eldeberky and Battjes* [1995] and *Eldeberky* [1996].

As for implicit propagation schemes, one type of implicit propagation scheme is piecewise wave ray propagation from one mesh of a computational grid to another [e.g., *Young*, 1988; *Yamaguchi*, 1990; *Benoit et al.*, 1996]. However, spatial variations in the driving fields (wind, bottom, and currents) over a distance of $c_g \Delta t$ are ignored during the integration along these characteristics (c_g is the energy propagation speed, and Δt is the integration time step). Since the grid is usually chosen to properly resolve these variations, $c_g \Delta t$ should still be smaller than the mesh size. This is equivalent to the Courant criterion for explicit schemes (now for reasons of accuracy rather than stability), and this approach is therefore not a reasonable alternative. The alternative that has been developed for SWAN is an implicit propagation scheme based on finite differences.

To validate both the propagation characteristics and the physical processes of generation and dissipation in SWAN, computational results are compared with (1) analytical solutions in academic cases, (2) laboratory observations, and (3) (generalized) field observations. The verification of SWAN with real field cases is described in a sequel paper [*Ris et al.*, this issue]. The paper is organized as follows. The basic formulations of the model are given in section 2. The numerical implementation and the related validations of the propagation schemes and of the source term integration are presented in section 3. A discussion with conclusions is given in section 4.

2. Model Formulation

2.1. Introduction

In SWAN the waves are described with the two-dimensional wave action density spectrum, even when nonlinear phenomena dominate (e.g., in the surf zone). The rationale for using the spectrum in such highly nonlinear conditions is that, even in such conditions, it seems possible to predict with reasonable accuracy this spectral distribution of the second-order moment of the waves (although it may not be sufficient to fully describe the waves statistically). The action density spectrum $N(\sigma, \theta)$ is considered rather than the energy density spectrum $E(\sigma, \theta)$ since in the presence of ambient currents, action density is conserved whereas energy density is not [e.g., *Whitham*, 1974]. The independent variables are the relative frequency σ (as

Table 1. Options of Third-Generation Source Terms in the Simulating Waves Nearshore Model

Source Term	Reference	SWAN		
		Added	WAM 3	WAM 4
Linear wind growth	<i>Cavaleri and Malanotte-Rizzoli</i> [1981]	x		
Exponential wind growth	<i>Komen et al.</i> [1984] <i>Janssen</i> [1991a]		xx	
Whitcapping	<i>Komen et al.</i> [1984] <i>Janssen</i> [1991a] and <i>Komen et al.</i> [1994]		xx	x
Quadruplet wave-wave interactions	<i>Hasselmann et al.</i> [1985]		xx	xx
Bottom friction	<i>Hasselmann et al.</i> [1973] <i>Collins</i> [1972] <i>Madsen et al.</i> [1988]	x x	xx	xx
Depth-induced breaking	<i>Battjes and Janssen</i> [1978]	xx		
Triad wave-wave interactions	<i>Eldeberky</i> [1996]	xx		

Options indicated as Wave Model (WAM) 3 and WAM 4 are the formulations also used in WAM cycle 3 and WAM cycle 4 models, respectively. Options that are available in SWAN are indicated by x. Preferred options in SWAN (default) are indicated by xx.

observed in a frame of reference moving with the current velocity) and the wave direction θ (the direction normal to the wave crest of each spectral component). The action density is equal to the energy density divided by this relative frequency, $N(\sigma, \theta) = E(\sigma, \theta)/\sigma$.

2.2. Action Balance Equation

The evolution of the wave spectrum is described by the spectral action balance equation, which, for Cartesian coordinates, is [e.g., *Hasselmann et al.*, 1973]

$$\frac{\partial}{\partial t} N + \frac{\partial}{\partial x} c_x N + \frac{\partial}{\partial y} c_y N + \frac{\partial}{\partial \sigma} c_\sigma N + \frac{\partial}{\partial \theta} c_\theta N = \frac{S}{\sigma} \quad (1)$$

The first term on the left-hand side of (1) represents the local rate of change of action density in time, the second and third term represent propagation of action in geographical space (with propagation velocities c_x and c_y in x and y space, respectively). The fourth term represents shifting of the relative frequency due to variations in depths and currents (with propagation velocity c_σ in σ space). The fifth term represents depth-induced and current-induced refraction (with propagation velocity c_θ in θ space). The expressions for these propagation speeds are taken from linear wave theory [e.g., *Whitham*, 1974; *Dingemans*, 1997]. The term S [= $S(\sigma, \theta)$] at the right-hand side of the action balance equation is the source term in terms of energy density, representing the effects of generation, dissipation, and nonlinear wave-wave interactions. A brief summary of the formulations that are used for the various processes in SWAN is given next, with an overview in Table 1. Details of the relatively new formulations for depth-induced breaking and triad wave-wave interactions are given in the appendix. The more established formulations for the other processes are well described in the following references.

2.3. Wind Input

Transfer of wind energy to the waves is described in SWAN with the resonance mechanism of *Phillips* [1957] and the feedback mechanism of *Miles* [1957]. The corresponding source term for these mechanisms is commonly described as the sum of linear and exponential growth:

$$S_m(\sigma, \theta) = A + BE(\sigma, \theta) \quad (2)$$

in which A and B depend on wave frequency and direction and wind speed and direction. The effects of currents are accounted for in SWAN by using the apparent local wind speed

and direction. The expression for the term A is due to *Cavaleri and Malanotte-Rizzoli* [1981] with a filter to avoid growth at frequencies lower than the *Pierson and Moskowitz* [1964] frequency [Tolman, 1992a]. Two optional expressions for the coefficient B are used in SWAN. The first is taken from an early version of the WAM model (known as WAM cycle 3 [WAMDI Group, 1988]). It is due to *Snyder et al.* [1981], rescaled in terms of friction velocity U_* by *Komen et al.* [1984]. The drag coefficient to relate U_* to the driving wind speed at 10 m elevation U_{10} is taken from *Wu* [1982]. The second expression for B in SWAN is taken from the most recent version of the WAM model (known as WAM cycle 4 [Komen et al., 1994]). It is due to *Janssen* [1991a], and it accounts explicitly for the interaction between the wind and the waves by considering atmospheric boundary layer effects and the roughness length of the sea surface. The corresponding set of equations is solved (as in the WAM model) with the iterative procedure of *Mastenbroek et al.* [1993].

2.4. Dissipation

The dissipation term of wave energy is represented by the summation of three different contributions: whitcapping $S_{ds,w}(\sigma, \theta)$, bottom friction $S_{ds,b}(\sigma, \theta)$, and depth-induced breaking $S_{ds,br}(\sigma, \theta)$. Whitcapping is primarily controlled by the steepness of the waves. In SWAN, as in other presently operating third-generation wave models, the whitcapping formulation is based on the pulse-based model of *Hasselmann* [1974], as adapted by the WAMDI Group [1988]:

$$S_{ds,w}(\sigma, \theta) = -\Gamma \bar{\sigma} \frac{k}{\bar{k}} E(\sigma, \theta) \quad (3)$$

where Γ is a steepness dependent coefficient, k is wave number, and $\bar{\sigma}$ and \bar{k} denote a mean frequency and a mean wave number, respectively [cf. WAMDI Group, 1988]. *Komen et al.* [1984] estimated the value of Γ by closing the energy balance of the waves in fully developed conditions. This implies that this value depends on the wind input formulation that is used. Since two expressions are used for the wind input in SWAN, two values for Γ are also used. The first is due to *Komen et al.* [1984] (as in cycle 3 of the WAM model). It is used in SWAN when the wind input coefficient B of *Komen et al.* [1984] is used. The second expression is an adaptation of this expression based on *Janssen* [1991a] (as in cycle 4 of the WAM model [see *Janssen*, 1991b; *Günther et al.*, 1992]). It is used when the wind input term B of *Janssen* [1991a] is used. *Young and Banner*

[1992] and *Banner and Young* [1994] have shown that the results of closing the energy balance in this manner depend critically on the choice of a high-frequency cutoff frequency, above which a diagnostic spectral tail is used. In SWAN this cutoff frequency is different from the one used in the WAM model. Differences in the growth rates between the WAM model and SWAN are therefore to be expected. This problem is addressed in section 3.3.2.

Bottom-induced dissipation may be caused by bottom friction, bottom motion, percolation, or backscattering on bottom irregularities [*Shemdin et al.*, 1978]. For continental shelf seas with sandy bottoms, the dominant mechanism appears to be bottom friction [e.g., *Bertotti and Cavaleri*, 1994], which can generally be represented as

$$S_{ds,b}(\sigma, \theta) = -C_{\text{bottom}} \frac{\sigma^2}{g^2 \sinh^2(kd)} E(\sigma, \theta) \quad (4)$$

in which C_{bottom} is a bottom friction coefficient. *Hasselmann et al.* [1973] (JONSWAP) used an empirically obtained constant. It seems to perform well in many different conditions as long as a suitable value is chosen (typically different for swell and wind sea [*Bouws and Komen*, 1983]). A nonlinear formulation based on drag has been proposed by *Hasselmann and Collins* [1968], which was later simplified by *Collins* [1972]. More complicated, eddy viscosity models have been developed by *Madsen et al.* [1988] (see *Weber* [1991a]) and *Weber* [1989, 1991a, b]. Considering the large variations in bottom conditions in coastal areas (bottom material, bottom roughness length, ripple height, etc.), there is no field data evidence to give preference to a particular friction model [*Luo and Monbaliu*, 1994]. For this reason, the simplest of each of these types of friction models has been implemented in SWAN: the empirical Joint North Sea Wave Project (JONSWAP) model of *Hasselmann et al.* [1973] (with $C_{\text{bottom}} = 0.038 \text{ m}^2 \text{ s}^{-3}$ for swell conditions and $C_{\text{bottom}} = 0.067 \text{ m}^2 \text{ s}^{-3}$ for wind sea conditions), the drag law model of *Collins* [1972] (with $C_{\text{bottom}} = C_f g U_{\text{rms}}$ with bottom friction coefficient C_f , gravitational acceleration g , and rms wave-induced orbital velocity at the bottom U_{rms}), and the eddy-viscosity model of *Madsen et al.* [1988] (with $C_{\text{bottom}} = f_w g U_{\text{rms}} / \sqrt{2}$ and f_w taken from *Jonsson* [1966, 1980] and *Jonsson and Carlsen* [1976]). The effect of a mean current on the wave energy dissipation due to bottom friction is not taken into account in SWAN. The reasons for this are given by *Tolman* [1992b], who argues that state-of-the-art expressions vary too widely in their effects to be acceptable. He found that the error in finding a correct estimate of the bottom roughness length scale has a much larger impact on the energy dissipation rate than the effect of a mean current.

The process of depth-induced wave breaking is still poorly understood and little is known about its spectral modeling. In contrast to this, the total dissipation (i.e., integrated over the spectrum) due to this type of wave breaking can be well modeled with the dissipation of a bore applied to the breaking waves in a random field [*Battjes and Janssen*, 1978; *Thornton and Guza*, 1983]. Laboratory observations [e.g., *Battjes and Beji*, 1992; *Vincent et al.*, 1994; *Arcilla et al.*, 1994; *Eldeberky and Battjes*, 1996] show that the shape of initially unimodal spectra propagating across simple (barred) beach profiles is fairly insensitive to depth-induced breaking. This has led *Eldeberky and Battjes* [1995] to formulate a spectral version of the bore model of *Battjes and Janssen* [1978], which conserves the spectral shape. Expanding their expression to include directions, the expression that is used in SWAN is

$$S_{ds,br}(\sigma, \theta) = -\frac{S_{ds,br,tot}}{E_{tot}} E(\sigma, \theta) \quad (5)$$

in which E_{tot} is the total wave energy and $S_{ds,br,tot}$ is the rate of dissipation of E_{tot} due to depth-induced wave breaking according to *Battjes and Janssen* [1978]. Adding a quadratic dependency on frequency as suggested by *Mase and Kirby* [1992] (supported by *Elgar et al.* [1997]) had no noticeable effect on the computed spectra of the present study. This agrees with the findings of *Chen et al.* [1997], who inferred from observations and simulations with a Boussinesq model that the high-frequency levels are insensitive to such frequency dependency because an increased dissipation at high frequencies is compensated approximately by increased nonlinear energy transfer (but they did find the frequency dependency to be relevant in time domain). The value of $S_{ds,br,tot}$ depends critically on the breaking parameter $\gamma = H_{\text{max}}/d$ (in which H_{max} is the maximum possible individual wave height in the local water depth d). In SWAN a constant value $\gamma = 0.73$ (the mean value of the data set of *Battjes and Stive* [1985]) and a variable value depending on the bottom slope [*Nelson*, 1987, 1994] are used. The appendix provides more details about this dissipation model.

2.5. Nonlinear Wave-Wave Interactions

In deep water, quadruplet wave-wave interactions dominate the evolution of the spectrum. They transfer wave energy from the spectral peak to lower frequencies (thus moving the peak frequency to lower values) and to higher frequencies (where the energy is dissipated by whitecapping). In very shallow water, triad wave-wave interactions transfer energy from lower frequencies to higher frequencies, often resulting in higher harmonics [*Beji and Battjes*, 1993] (low-frequency energy generation by triad wave-wave interactions is not considered here).

A full computation of the quadruplet wave-wave interactions is extremely time consuming and not convenient in any operational wave model. A number of techniques, based on parametric methods or other types of approximations, have been proposed to improve computational speed (see *Young and Van Vledder* [1993] for a review). In SWAN the computations are carried out with the discrete interaction approximation of *Hasselmann et al.* [1985]. This DIA has been found quite successful in describing the essential features of a developing wave spectrum [*Komen et al.*, 1994]. For unidirectional waves (such as used in some of the validation tests of SWAN; see section 3.3.2) this approximation is not valid. In fact, the quadruplet interaction coefficient for these waves is nearly zero (G. P. Van Vledder, personal communication, 1996). For finite-depth applications, *Hasselmann and Hasselmann* [1981] have shown that for a JONSWAP-type spectrum the quadruplet wave-wave interactions can be scaled with a simple expression (it is used in SWAN).

A first attempt to describe triad wave-wave interactions in terms of a spectral energy source term was made by *Abreu et al.* [1992]. However, their expression is restricted to nondispersive, shallow-water waves and is therefore not suitable in many practical applications of wind waves. A breakthrough came with the work of *Eldeberky and Battjes* [1995] to provide SWAN with an economically feasible formulation of the triad wave-wave interactions. They transformed the amplitude part of the Boussinesq model of *Madsen and Sørensen* [1993] into an energy density formulation, and they parameterized the biphase of the waves on the basis of laboratory observations [*Battjes*

and Beji, 1992; Arcilla *et al.*, 1994]. A discrete triad approximation (DTA) for collinear waves was subsequently obtained by considering only the dominant self-self interactions. Their formulation has been verified with flume observations of long-crested, random waves breaking over a submerged bar [Beji and Battjes, 1993] and over a barred beach [Arcilla *et al.*, 1994]. The formulation appeared to be fairly successful in describing the essential features of the energy transfer from the primary peak of the spectrum to the superharmonics. A slightly different version (the lumped triad approximation (LTA)) was later derived by Eldeberky [1996]. Details on this LTA as used in SWAN are provided in the appendix.

3. Model Implementation and Validation

3.1. Introduction

The integration of the action balance equation has been implemented in SWAN with finite difference schemes in all five dimensions (time, geographic space, and spectral space). These are first described and validated for the propagation of the waves without source terms. Then the implementation of the source terms is described and validated.

In SWAN, time is discretized with a simple constant time step Δt for the simultaneous integration of the propagation and the source terms. This is different from the time discretization in the WAM model or the WAVEWATCH model, where the time step for propagation is different from the time step for the source terms. Geographic space is discretized with a rectangular grid with constant resolutions Δx and Δy in the x and y direction, respectively. The spectrum in SWAN is discretized with a constant directional resolution $\Delta\theta$ and a constant relative frequency resolution $\Delta\sigma/\sigma$ (logarithmic frequency distribution). For reasons of economy an option is available to compute only wave components traveling in a predefined directional sector ($\theta_{\min} < \theta < \theta_{\max}$, e.g., those components that travel shoreward within a limited directional sector). The discrete frequencies are defined between a fixed low-frequency cutoff and a fixed high-frequency cutoff (the prognostic part of the spectrum). For these frequencies the spectral density is unconstrained. Below the low-frequency cutoff (typically, $f_{\min} = 0.04$ Hz for field conditions) the spectral densities are assumed to be zero. Above the high-frequency cutoff (typically, 1 Hz for field conditions) a diagnostic f^{-m} tail is added (this tail is used to compute nonlinear wave-wave interactions at high frequencies and to compute integral wave parameters). The reason for using a fixed high-frequency cutoff rather than a dynamic cutoff frequency that depends on the wind speed or on the mean frequency, as in the WAM model, is that in coastal regions, mixed sea states with rather different characteristic frequencies may occur. For instance, a local wind may generate a very young sea behind an island, totally unrelated to (but superimposed on) a simultaneously occurring swell. In such cases a dynamic cutoff frequency may be too low to properly account for the locally generated sea state. On the basis of physical arguments, the value of m (the power in the above expression of the spectral tail) should be between 4 and 5 [e.g., Phillips, 1985]. In SWAN, $m = 4$ if the wind input formulation of Komen *et al.* [1984] is used (WAM cycle 3) and $m = 5$ if the wind input formulation of Janssen [1991a] is used (WAM cycle 4).

3.2. Propagation

3.2.1. Implementation of propagation. The numerical propagation schemes in SWAN are implicit schemes that have not been used before in other wave models (although a simple

version was used in the second-generation Hindcasting Shallow Water Waves (HISWA) wave model of Holthuijsen *et al.* [1989]. They have been chosen on the basis of robustness, accuracy, and economy.

Since the nature of the action balance equation is such that the state in a grid point is determined by the state in the upwave grid points, the most robust scheme would be an implicit upwind scheme (in both geographic and spectral space). The adjective “implicit” is used here to indicate that all derivatives of action density (in t , x , or y) are formulated at one computational level, i_t , i_x , or i_y , except the derivative in the integration dimension for which also the previous or upwave level is used (time and x or y , depending on the direction of propagation). For such a scheme the values of the time and space steps Δt , Δx , and Δy are mutually independent. An implicit scheme is also economical in the sense that such a scheme is unconditionally stable. It permits relatively large time steps in the computations (much larger than for explicit schemes in shallow water). Several years of experience in using the HISWA model have shown that for coastal regions a first-order upwind difference scheme in geographic space is usually accurate enough. However, this experience, together with test computations with SWAN, has also shown that in spectral space a higher accuracy than that of a first-order upwind scheme is required. This has been achieved by supplementing the scheme with a second-order central approximation (more economic than a second-order upwind scheme). For SWAN therefore implicit upwind schemes in both geographic and spectral space have been chosen, supplemented with an implicit central approximation in spectral space.

The fact that in geographic space the state in a grid point is determined by the state in the upwave grid points (as defined by the direction of propagation) permits a decomposition of the spectral space into four quadrants (eight octants would be an alternative). In each of the quadrants the computations can be carried out independently from the other quadrants, except for the interactions between them due to refraction and nonlinear source terms (corresponding to boundary conditions between the quadrants). The wave components in SWAN are correspondingly propagated in geographic space with the first-order upwind scheme in a sequence of four forward marching sweeps (one per quadrant). To properly account for the boundary conditions between the four quadrants, the computations are carried out iteratively at each time step. The integration in time is a simple backward finite difference, so that the discretization of the action balance equation is (for positive propagation speeds, including the computation of the source terms but ignoring their discretization)

$$\begin{aligned}
 & \left[\frac{N^{i_t, n} - N^{i_t-1, n}}{\Delta t} \right]_{i_x, i_y, i_\sigma, i_\theta} + \left[\frac{[c_x N]_{i_x} - [c_x N]_{i_x-1}}{\Delta x} \right]_{i_y, i_\sigma, i_\theta}^{i_t, n} \\
 & + \left[\frac{[c_y N]_{i_y} - [c_y N]_{i_y-1}}{\Delta y} \right]_{i_x, i_\sigma, i_\theta}^{i_t, n} \\
 & + \left[\frac{(1 - \nu)[c_\sigma N]_{i_\sigma+1} + 2\nu[c_\sigma N]_{i_\sigma} - (1 + \nu)[c_\sigma N]_{i_\sigma-1}}{2\Delta\sigma} \right]_{i_x, i_y, i_\theta}^{i_t, n} \\
 & + \left[\frac{(1 - \eta)[c_\theta N]_{i_\theta+1} + 2\eta[c_\theta N]_{i_\theta} - (1 + \eta)[c_\theta N]_{i_\theta-1}}{2\Delta\theta} \right]_{i_x, i_y, i_\sigma}^{i_t, n} \\
 & = \left[\frac{S}{\sigma} \right]_{i_x, i_y, i_\sigma, i_\theta}^{i_t, n*} \quad (6)
 \end{aligned}$$

where i_t is the time level index; i_x , i_y , i_σ , and i_θ are grid counters; and Δt , Δx , Δy , $\Delta \sigma$, and $\Delta \theta$ are the increments in time, geographic space, and spectral space, respectively. The iterative nature of the computation is indicated with the iteration index n (the iteration index for the source terms n^* is equal to n or $n-1$, depending on the source term; see below). Because of these iterations, the scheme is also approximately implicit for the source terms (see section 3.3.1). For negative propagation speeds, appropriate plus and minus signs are required in (6).

The coefficients ν and η determine the degree to which the scheme in spectral space is upwind or central. They thus control the numerical diffusion in frequency and directional space, respectively. A value of $\nu = 0$ or $\eta = 0$ corresponds to central schemes which have the largest accuracy (numerical diffusion ≈ 0). A value of $\nu = 1$ or $\eta = 1$ corresponds to upwind schemes, which are somewhat more diffusive and therefore less accurate but more robust. In the present study all computations are carried out with $\nu = \eta = 1/2$. If large gradients of the action density in frequency space or directional space are present, numerical oscillations can arise (especially with the central difference schemes), resulting in negative values of the action density. In each sweep such negative values are removed from the two-dimensional spectrum by setting these values equal to zero and rescaling the remaining positive values such that the frequency-integrated action density per spectral direction is conserved. The depth derivatives and current derivatives in the expressions of c_σ and c_θ are calculated with a first-order upwind scheme.

For stationary conditions, SWAN can be run in stationary mode. Time is then removed as a variable, but the integration (in geographic space) is still carried out iteratively. The propagation scheme is still implicit, as the derivatives of action density (in x or y) at the computational level (i_x or i_y , respectively) are formulated at that level, except in the integration dimension (x or y , depending on the direction of propagation), where the upwave level is also used. The values of Δx and Δy are therefore still mutually independent.

To explain the above numerical solution technique in terms of matrix solutions, first ignore the decomposition in quadrants. The propagation of the waves in both geographic and spectral space would then be described with one large basic matrix that can be solved in several ways. Removing refraction, frequency shifting, and nonlinear source terms from this basic matrix permits a matrix solution with a Gauss-Seidel technique [e.g., Golub and van Loan, 1986] in which the matrix is decomposed in four sections (the above four directional quadrants), which are each solved in one step (superconvergence). Restoring refraction and frequency shifting to the matrix requires the solution of a submatrix for each geographic grid point. If no currents are present and the depth is stationary, this is readily done with a Thomas algorithm [e.g., Abbott and Basco, 1989] ($c_\sigma = 0$ and the submatrix is a simple tridiagonal matrix). If currents are present or the depth is not stationary, the submatrix is a band matrix. It is solved with an iterative Incomplete Lower and Upper Triangular Matrix Decomposition-Bi-Conjugate Gradient Stabilized (ILU-BiCGSTAB) method [Vuik, 1993; Van der Vorst, 1992]. Restoring refraction and frequency shifting also introduces coefficients in each matrix section (directional quadrant) that cause dependency between the matrix sections. The same happens when nonlinear source terms are added to the matrix. The basic matrix as a whole

needs therefore to be solved iteratively until some break-off criteria are met.

In the field cases of the present study (this paper and *Ris et al.*, this issue], the break-off criteria are as follows: in more than 97% of the submerged grid points the change in significant wave height [$H_s = 4\sqrt{m_0}$, where $m_n = \int \sigma^n E(\sigma) d\sigma$] from one iteration to the next is less than 3% or 0.03 m and, also, the change in the mean relative wave period ($T_{m01} = 2\pi m_0/m_1$) is less than 3% or 0.3 s. For laboratory cases, stricter criteria are used.

The number of iterations for cases with wave generation by wind is typically 5–15 in the present study (stationary cases in which the iterations start from totally calm sea). For the academic cases, stricter criteria were used to verify the convergence to the proper analytical solutions (e.g., the break-off criterion for the significant wave height was 0.1%) and the number of iterations was typically 30–40. For all these computations the convergence was monotonic, although extending the computations beyond the break-off criteria showed that occasionally, the solution continued with fluctuations that were somewhat smaller than the break-off criterion. To reduce the number of iterations in stationary mode with wind generation, the computations that are shown in this paper and in the sequel paper [*Ris et al.*, this issue] start with a reasonable first guess of the wave field (a “quick start” based on the second-generation source terms of *Holthuijsen and De Boer* [1988], adapted for shallow water). It reduces the number of iterations mentioned above typically by a factor of 2 (i.e., three to seven iterations). In nonstationary mode a reasonable first guess per time step is available from the previous time step and the number of iterations is expected to be small (less than 4). If no iterations are used in nonstationary mode (as in most other phase-averaged wave models), the computations of propagation are still implicit and therefore still unconditionally stable.

The boundary conditions in SWAN, both in geographic space and spectral space, are fully absorbing for wave energy that is leaving the computational domain or crossing a coastline. The incoming wave energy along open geographic boundaries needs to be prescribed by the user. For coastal regions such incoming energy is usually provided only along the deepwater boundary and not along the lateral geographic boundaries (that is, the spectral densities are assumed to be zero). This implies that such erroneous lateral boundary conditions are propagated into the computational area. The affected areas are typically triangular regions with the apex at the corners between the deepwater boundary and the lateral boundaries, spreading toward shore at an angle of 30° to 45° (for wind sea conditions) on either side of the deepwater mean wave direction (less for swell conditions; this angle is essentially half the total width of the directional distribution of the incoming wave spectrum). For this reason, the lateral boundaries should be sufficiently far away from the area of interest to avoid the propagation of this error into the area of interest.

3.2.2. Tests of propagation. Ideally, the propagation scheme in SWAN should be free of numerical diffusion. However, for long propagation distances (oceanic scales) the diffusion for the first-order implicit schemes of SWAN is fairly large; but, since SWAN is primarily a coastal wave model with short propagation distances, the integrative effect of the diffusion seems to be acceptable. A full analysis of the diffusion in both geographic and spectral space is fairly complicated and beyond the scope of this study (the diffusion coefficients in-

volve combinations of propagation speeds and increment sizes in the five dimensions, t , x , y , σ , and θ).

For the stationary mode of SWAN a rough theoretical estimate of the diffusion is readily made in geographic space for constant depth and no currents [e.g., Roache, 1972]. The coefficient for diffusion in the y direction is

$$D_y = \frac{1}{2} \left[\left(\frac{c_x}{c_y} \right)^2 \Delta y + \frac{c_x}{c_y} \Delta x \right] \quad (7)$$

To verify that SWAN properly reproduces this theoretically estimated diffusion, the model is used (without source terms) in stationary mode for a harmonic, long-crested wave propagating in deep water through a $150(2)^{1/2}$ m wide gap at an angle of 45° with the positive x axis (Figure 1). The (significant) wave height in the gap is 1 m, and the frequency is 0.1 Hz. The analytical estimate of the diffusive spreading in the y direction (spatial standard deviation $\sigma_y = (2D_y x)^{1/2}$) is shown in Figure 1. In the SWAN computation this harmonic wave is simulated with a Gaussian-shaped frequency spectrum with peak frequency 0.1 Hz, standard deviation 0.01 Hz, and a resolution of 3% of the frequency (diffusion in frequency space does not occur as $c_\sigma = 0$ in this case, and the frequency resolution may therefore be somewhat coarse). The long crestedness in this computation is simulated with a $\cos^{500}(\theta)$ directional distribution (the directional width $\sigma_\theta = 2.5^\circ$, where σ_θ is the standard deviation of the directional distribution, defined by Kuik et al. [1988], averaged over all frequencies weighted with the spectral densities). The resolutions Δx and Δy are both 100 m, and the directional resolution is 0.5° . The spreading of these waves (which are not perfectly long crested) is $\sigma_y = [2D_y x + (2x \tan \sigma_\theta)^2]^{1/2}$. The agreement between this solution and the computational results is shown in Figure 1 (error in σ_y less than 0.5%). Note that the wave direction remains constant since in deep water, $c_\theta = 0$ and no diffusion occurs in θ space.

To test the propagation scheme in the presence of an ambient current, consider the same waves propagating in deep water from a uniform upwave boundary over a distance of 4000 m in a following current or an opposing current of which the speed U increases from 0 to 2 m s^{-1} in the downwave direction (current direction 0° or 180° relative to the wave direction). The analytical solution for this case is given by Phillips [1977] and Jonsson [1993]

$$\frac{H^2}{H_i^2} = \frac{c_i^2}{c(c + 2U)} \quad (8)$$

$$\frac{c}{c_i} = \frac{1}{2} + \frac{1}{2} \left(1 + 4 \frac{U}{c_i} \right)^{1/2} \quad (9)$$

in which H and c are the wave height and group velocity, respectively, and the subscript i denotes the incident value. Note that the wave direction remains constant since $c_\theta = 0$ (no refraction). This solution is shown in Figure 2, where the computational results are also shown in terms of (significant) wave height (same resolutions and long crestedness as in the above diffusion test, except that the resolution in x direction is 40 m and the frequency resolution is 1%). Current-induced refraction (deep water) is readily tested by turning the ambient current direction over 90° (each vector in the current field, not the field as a whole) and the incident waves over 30° (positive or negative). The analytical solution for such a case is [e.g., Hedges, 1987; Jonsson, 1993]

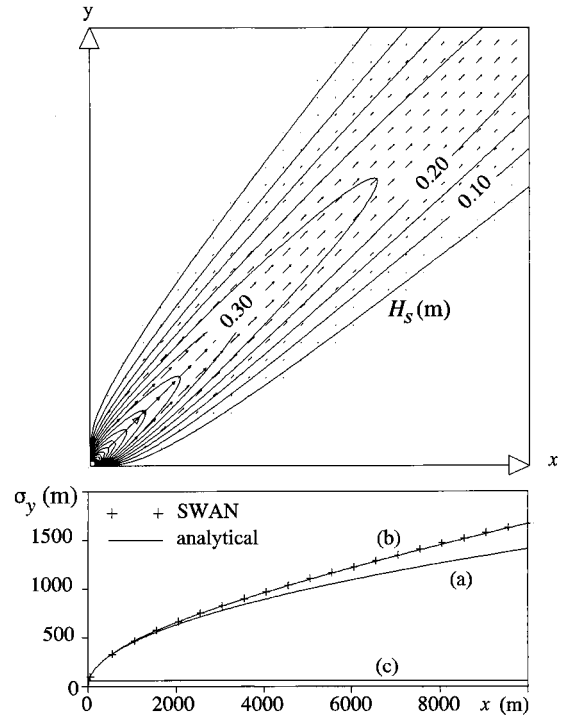


Figure 1. Numerical diffusion in geographical space. (top) Computational area ($10 \text{ km} \times 10 \text{ km}$), isolines of the significant wave height H_s with interval 0.05 m. Vectors represent the mean direction and magnitude of energy transport. (bottom) Spreading of the wave field expressed as the width of the spatial distribution in the y direction. Lines represent analytical solutions for long-crested waves, with numerical diffusion (labeled a), with numerical diffusion and $\cos^{500}(\theta)$ directional distribution (labeled b), and no diffusion (labeled c). Crosses represent the Simulating Waves Nearshore (SWAN) model results (only with numerical diffusion and $\cos^{500}(\theta)$ directional distribution).

$$H = H_i \sqrt{\frac{\sin(2\theta_i)}{\sin(2\theta)}} \quad (10)$$

$$\theta = \arccos \left[\frac{gk_i \cos(\theta_i)}{(\omega - Uk_i \cos(\theta_i))^2} \right] \quad (11)$$

This analytical solution is also shown in Figure 2 with the results of the SWAN computations in terms of (significant) wave height (same resolutions and long crestedness as in the above propagation test). For all four of these propagation tests with ambient currents, the computational errors are small (less than 0.5% for the significant wave height and less than 0.1° for the wave direction).

To test the propagation scheme in shallow water with varying depth (depth-induced shoaling and refraction without currents), consider the same waves propagating over a distance of 4000 m toward a plane beach from 20-m water depth (slope 1:200). Shoaling is readily tested by propagating the waves perpendicularly to the shore. Depth-induced refraction is readily added by turning the incident wave direction over 30° . The analytical solution of linear wave theory in terms of wave height is given by

$$\frac{H^2}{H_i^2} = \frac{c_i \cos(\theta_i)}{c \cos(\theta)} \quad (12)$$

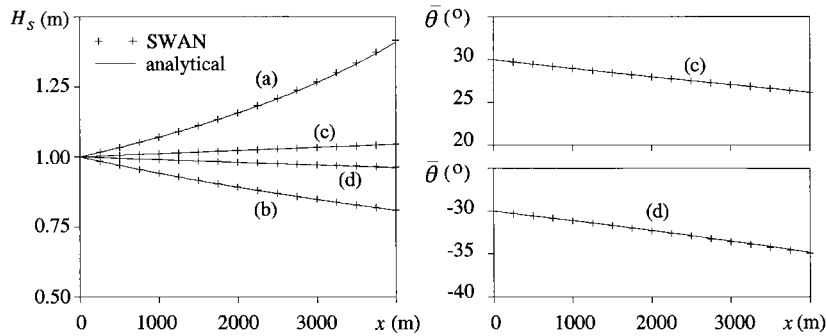


Figure 2. Current-induced shoaling and refraction for monochromatic, long-crested waves. (left) Significant wave height H_s . (right) Mean wave direction $\bar{\theta}$. Lines represent analytical solutions for waves traveling against an opposing current (no refraction) (labeled a), with a following current (no refraction) (labeled b), (c) across a slanting current with incident wave direction $\bar{\theta}_o = 30^\circ$ (labeled c), and across a slanting current with incident wave direction $\bar{\theta}_o = -30^\circ$ (labeled d). Crosses represent the SWAN results.

where the wave direction is calculated with Snell's law. This analytical solution is shown in Figure 3, where the results of the SWAN computations are also shown in terms of (significant) wave height (same resolutions and long crestedness as in the above propagation test). The agreement with linear theory is again good. The errors are less than 0.1% in significant wave height and less than 0.25° in direction (for depths larger than 0.05 m).

3.3. Generation, Wave-Wave Interactions, and Dissipation

3.3.1. Implementation of source terms. The numerical estimations of the source terms in SWAN are essentially implicit. This is achieved with explicit or implicit approximations of the source terms, which in the limit of a large number of iterations (see section 3.2.1) are always implicit. In actual computations, final convergence is obviously never achieved and the estimations of the source terms are therefore, strictly speaking, only approximately implicit. In the following the adjectives “explicit” and “implicit” refer to the approximations of the source terms within each iteration.

The linear growth term A is independent of integral wave parameters and the energy density and can therefore be readily computed. All other source terms depend on energy density, and they can be described as a (quasi-)linear term: $S = \phi E$, in which ϕ is a coefficient that depends on (integral) wave parameters (e.g., E_{tot} , $\bar{\sigma}$, \bar{k} , σ , k , etc.) and action densities of

other spectral components. Since these are only known at the previous iteration level $n-1$, the coefficient ϕ is determined at that iteration level: $\phi = \phi^{n-1}$.

For positive source terms (wind input and the triad and quadruplet wave-wave interactions if positive) the integration is generally more stable if an explicit formulation is used (i.e., the source term depends on E^{n-1} and not on E^n) rather than an implicit formulation (i.e., the source term depends also on E^n). The explicit formulation for these source terms in SWAN is therefore

$$S^n \approx \phi^{n-1} E^{n-1} \quad (13)$$

For reasons of economy this explicit approximation is also used for the formulation of the quadruplet wave-wave interactions if negative. This is considered reasonable since Tolman [1992a] has shown that using an explicit formulation in combination with a limiter (see below) gives results similar to those of a more expensive implicit scheme (this implicit formulation is also optionally available in SWAN; in the WAM model it is indicated as the semi-implicit scheme [WAMDI Group, 1988; Komen et al., 1994]).

For negative source terms the integration is generally more stable if an implicit scheme is used. The strongly nonlinear, negative source term of depth-induced wave breaking at iteration level n is accordingly estimated with a linear approximation:

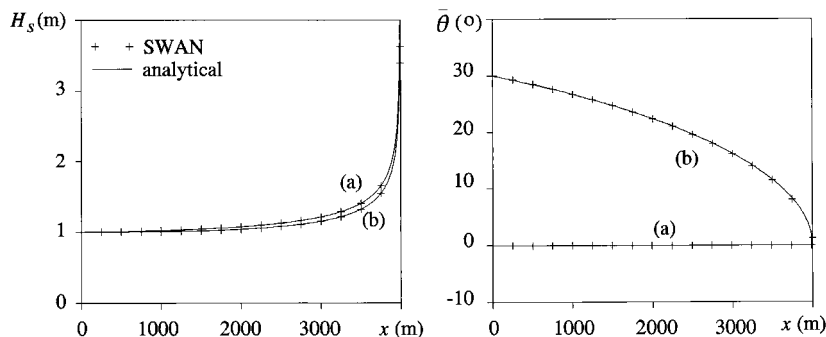


Figure 3. Depth-induced shoaling and refraction for monochromatic, long-crested waves on a plane beach (slope 1:200). (left) Significant wave height H_s . (right) Mean wave direction $\bar{\theta}$. Lines represent analytical solutions for incident wave direction $\bar{\theta}_o = 0^\circ$ (labeled a) and incident wave direction $\bar{\theta}_o = 30^\circ$ (labeled b). Crosses represent the SWAN results.

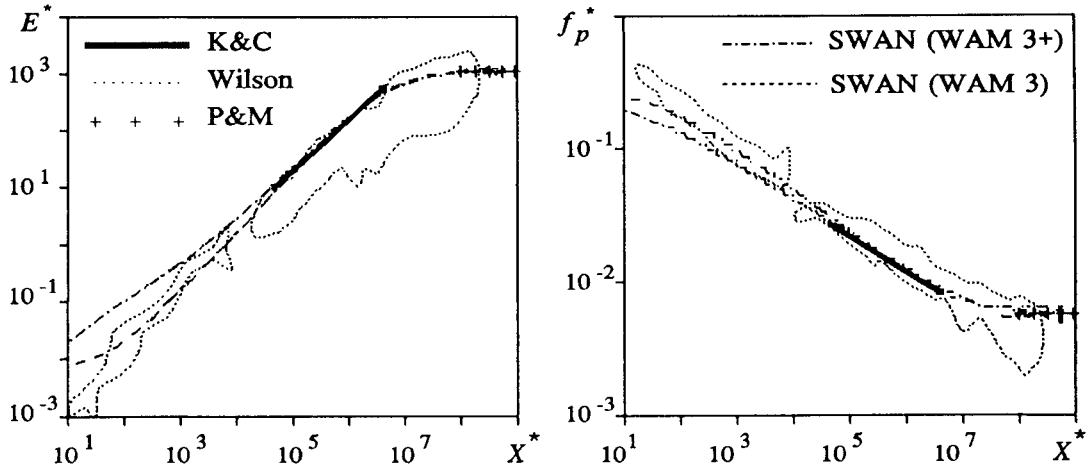


Figure 4. Deepwater fetch-limited growth of (left) nondimensional energy E^* and (right) nondimensional peak frequency f_p^* as a function of nondimensional fetch X^* . Analytical expression of *Kahma and Calkoen* [1992] (K&C), envelope of observations of *Wilson* [1965], and limit values of *Pierson and Moskowitz* [1964] (P&M) are included. Dashed lines represent SWAN results with WAM cycle 3 formulations, indicated as SWAN (WAM 3), and with the added linear growth term, indicated as SWAN (WAM 3+). The wind speed is $U_{10} = 20 \text{ m s}^{-1}$.

$$S^n \simeq \Phi^{n-1} E^{n-1} + \left(\frac{\partial S}{\partial E} \right)^{n-1} (E^n - E^{n-1}). \quad (14)$$

However, to achieve even more stable computations for this source term, the term $\phi^{n-1} E^{n-1}$ in this formulation has been replaced by $\phi^{n-1} E^n$ (making the formulation somewhat more implicit and thus more robust; note that in the limit the solution is the same). Since this process of depth-induced wave breaking has been formulated such that $S = a S_{\text{tot}}$ and $E = a E_{\text{tot}}$ (where a is identical in both expressions; see the appendix), the derivative $\partial S / \partial E$ is analytically determined as $\partial S_{\text{tot}} / \partial E_{\text{tot}}$ (where the total energy E_{tot} and the total source S_{tot} are the integrals over all frequencies and directions of $E(\sigma, \theta)$ and $S_{ds,br}(\sigma, \theta)$, respectively). For the other (mildly nonlinear) negative source terms, i.e., whitecapping, bottom friction, and negative triad wave-wave interactions, a similar accuracy of estimating S^n can be achieved with the following simpler and therefore more economical approximation in which $(\partial S / \partial E)^{n-1}$ of (14) has been replaced by $(S/E)^{n-1}$

$$S^n \simeq \Phi^{n-1} E^{n-1} + \left(\frac{S}{E} \right)^{n-1} (E^n - E^{n-1}). \quad (15)$$

With $S = \phi E$, this reduces to

$$S^n \simeq \Phi^{n-1} E^n. \quad (16)$$

These approximations for the source terms are added to the elements of the matrix for propagation. To suppress the development of numerical instabilities, the maximum total change of action density per iteration at each discrete wave component is limited to a fraction of 10% of the *Phillips* [1957] equilibrium level (reformulated in terms of action density and wave number to be applicable in shallow water, as in the WAM model and in the WAVEWATCH model [Tolman, 1992a]:

$$|\Delta N(\sigma, \theta)|_{\text{max}} = \frac{0.1}{2\pi\sigma} \frac{\alpha_{\text{PM}}\pi}{k^3 c_g} \quad (17)$$

where $\alpha_{\text{PM}} = 0.0081$ is the Phillips' "constant" of the *Pierson and Moskowitz* [1964] spectrum. To retain the very rapid but realistic decrease of wave energy near the shore due to depth-induced wave breaking, this limiter is not applied if the waves actually break (in SWAN, $H_{\text{max}}/H_{\text{rms}} > 0.5$, with $H_{\text{rms}} = (8E_{\text{tot}})^{1/2}$, which implies a fraction of breakers $Q_b > 0.00001$; see the appendix).

3.3.2. Tests of source terms. In the following the source terms are tested by comparing computational results with (generalized) observations. Since usually more than one formulation is available in SWAN for each source term, these tests will be used to select the formulation that provides the best agreement with these observations. The flexibility of SWAN in this respect is therefore used here to find the optimum choice of source term formulation (within the scope of the available options).

To test the deepwater generation of the waves in SWAN, consider an idealized case of a constant wind blowing perpendicularly off a long and straight coastline. The dimensionless total wave energy $E^* = g^2 E_{\text{tot}} / U_*^4$ and dimensionless peak frequency $f_p^* = U_* f_p / g$ (where f_p is the peak frequency) as a function of dimensionless fetch $X^* = gX / U_*^2$ (where X is the fetch) are given in Figure 4 for wind speed $U_{10} = 20 \text{ m s}^{-1}$ computed with the WAM cycle 3 formulations, with and without linear growth added. A scaling with the friction velocity U_* has been chosen here because the WAM formulations should scale with U_* . The expression of *Wu* [1982] for converting U_{10} into U_* has been used wherever relevant. The expression of *Kahma and Calkoen* [1992] and the limit value of *Pierson and Moskowitz* [1964] (as converted by *Komen et al.* [1984] in terms of U_* instead of the original $U_{19.5}$) are also given. To extend the observational information to very short fetches (for wind generation behind barrier islands), the envelope of the data compiled by *Wilson* [1965, Figure 15] is added (for the conversion of his dimensionless parameters an average wind speed in his observations of $U_{10} = 15 \text{ m s}^{-1}$ is assumed). Figure 4

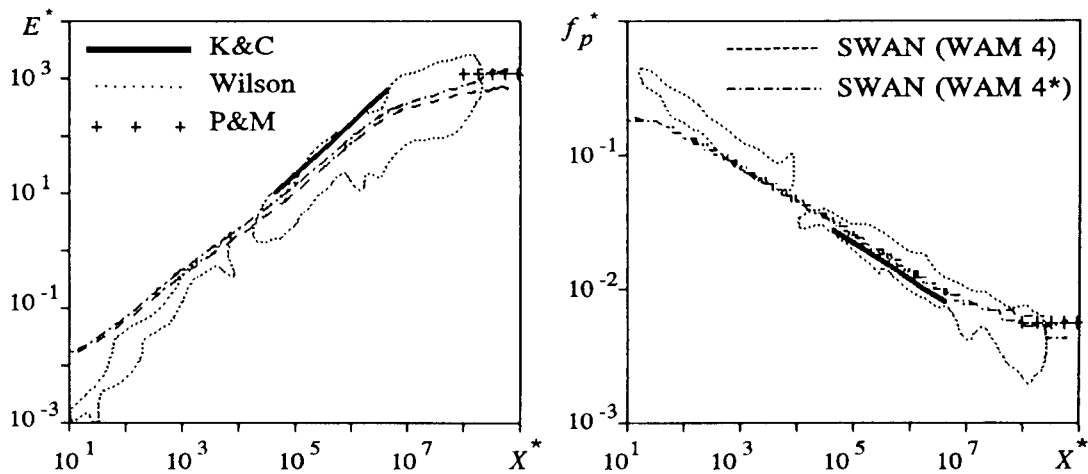


Figure 5. Same as Figure 4, except with WAM cycle 4 formulations used. Lines represent the computations with the original coefficient of *Janssen* [1991b] ($C_{ds} = 4.5$), indicated as SWAN (WAM 4) and with the retuned coefficient ($C_{ds} = 3.0$), indicated as SWAN (WAM 4*).

shows that the agreement is good between the SWAN results on the one hand and the expressions of *Kahma and Calkoen* [1992] and the limit values of *Pierson and Moskowitz* [1964] on the other. However, for very short fetches ($X^* < 10^4$, say) the model with linear growth added overestimates the total energy and, correspondingly, underestimates the peak frequency as compared with the data of *Wilson* [1965]. This overestimation, respectively, underestimation, at very small fetches is ascribed to the linear growth term A because at very short fetches the low frequencies show relatively high levels of energy (incompatible with the shape of the JONSWAP spectrum [*Hasselmann et al.*, 1973]). A possible reason is that the expression of *Cavaleri and Malanotte-Rizzoli* [1981] is used for all spectral components (above the *Pierson and Moskowitz* [1964] frequency), whereas it is strictly valid only near the resonance frequencies (varying with spectral direction). Removing this linear growth improves the agreement over a much larger range of fetches, as shown in Figure 4. For this reason, the linear growth is omitted in the following (but not in the first-guess start of the stationary mode of SWAN; in the nonstationary mode a low initial sea state is assumed).

As noted earlier, the results of *Young and Banner* [1992] suggest that some effects are to be expected of using a fixed cutoff frequency in SWAN rather than a dynamic cutoff frequency as in the WAM model. However, the above agreement with the observations suggests no such sensitivity in SWAN (at least not for the WAM cycle 3 formulations). A possible explanation is that *Young and Banner* [1992] used other approximations for the wind input and for computing the quadruplet wave-wave interactions (*Yan* [1987] and *Resio and Perrie* [1991], respectively).

The deepwater growth curves of SWAN as computed with the WAM cycle 4 formulations (without the linear growth term) for a wind speed of $U_{10} = 20 \text{ m s}^{-1}$ are shown in Figure 5. In contrast to the results with the WAM cycle 3 formulations, these results do not agree well with the generalized observations. Again, this may be due to the use of a fixed cutoff frequency rather than a dynamic cutoff frequency. One indication of this is that changing the cutoff frequency in the WAM cycle 4 formulations from 1 to 1.5 Hz increases the significant wave height in the fully developed situation by 16%, whereas it

increases only 5% when the WAM cycle 3 formulations are used. This is consistent with the findings of *Tolman* [1992a]. To achieve a better agreement with the *Pierson and Moskowitz* [1964] limit values, the coefficient C_{diss} in the expression for whitecapping of *Janssen* [1991b] ($C_{diss} = 4.5$, *Janssen's* notation) was retuned with the results that $C_{diss} = 3.0$ (remarkably close to the value of 2.6 as initially used by *Janssen* [1991a]). The required *Pierson and Moskowitz* [1964] limit values were thus obtained (see Figure 5), but (1) the total energy is significantly overestimated at very short fetches and underestimated at larger fetches, (2) the peak frequency is correspondingly significantly underestimated at short fetches (but not at very large fetches), and (3) spurious oscillations are introduced at (very) large fetches. In view of this rather poor agreement, only the WAM cycle 3 formulations are used in the following.

Figure 6 shows some of the spectra computed with SWAN in the above case with WAM cycle 3 formulations. The overshoot is not as pronounced as in observations (e.g., during JONSWAP [*Hasselmann et al.*, 1973]) or computed with exact computations of the quadruplet wave-wave interactions [*Hasselmann and Hasselmann*, 1981; *SWAMP Group*, 1985]. This result is similar to that of the WAM model with its cycle 3 formulations [see *Komen et al.*, 1984].

To test the implementation of the triad wave-wave interactions (the LTA formulation of *Eldeberky* [1996]), consider a one-dimensional case in which the waves propagate from deep water over a submerged bar without breaking but with the generation of a significant, secondary high-frequency peak in the spectrum. This situation has been observed *Beji and Battjes* [1993] in a flume (Figure 7). In the SWAN computations the observed spectrum is imposed at the first wave gauge 1 (i.e., a JONSWAP spectrum with a significant wave height of $H_s = 0.02 \text{ m}$ and a peak frequency of $f_p = 0.50 \text{ Hz}$). The long-crestedness is simulated as before with a $\cos^{500}(\theta)$ directional distribution, and the computations are carried out without quadruplet wave-wave interactions (see section 2.5). It was verified that the computational results are insensitive to bottom friction and depth-induced breaking in the computations. The computational results shown in Figure 8 agree well with the observations. However, the evolution of the secondary peak is fairly insensitive for the value of the proportionality

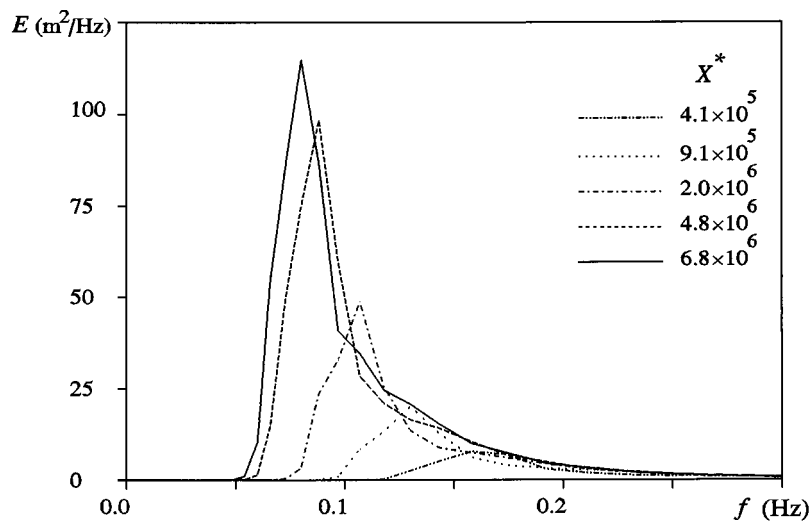


Figure 6. Deepwater wave spectra at various dimensionless fetches computed by SWAN with WAM cycle 3 formulations. The wind speed is 20 m s^{-1} .

coefficient α_{EB} in the expression of *Eldeberky* [1996] (see (A7)), which was varied between 0.125 and 0.5 (see Figure 8). This is probably due to the fact that the shape of the observed spectra over the bar is practically an equilibrium shape for triad wave-wave interactions in the expression of *Eldeberky* [1996] (the interactions in the LTA formulation are zero when the spectral level at the base frequency is twice the spectral level of its second harmonic). On the other hand, the evolution of the primary peak is sensitive to variations in α_{EB} and the results suggest that, in this respect, a compromise is obtained with $\alpha_{EB} = 0.25$. This value is therefore used in all following computations.

To test the implementation of depth-induced breaking, consider a one-dimensional case in which the waves propagate from deep water into shallow water to the beach across a bar-trough profile with violent wave breaking. This situation has been observed by *Battjes and Janssen* [1978] in another flume (Figure 9). The incident wave spectrum in this experiment is a JONSWAP spectrum with significant wave height 0.20 m and a peak frequency 0.53 Hz. The long crestedness is simulated as before with a $\cos^{500}(\theta)$ directional distribution, and for the same reason as above, the computations are carried out without quadruplet wave-wave interactions (but with triad wave-wave interactions). Again, bottom friction was verified to be insignificant. The results of the computations are given in Figure 9 for the constant breaker parameter $\gamma = 0.73$ of *Battjes and Stive* [1985] and the (clipped) variable breaker parameter γ of *Nelson* [1987, 1994] (also (A5)). The agreement between

the observations and the computed results is good for both formulations with nearly identical results. The constant value of $\gamma = 0.73$ is used in the following.

To test bottom friction, consider the generation of waves in an idealized situation in shallow water. The situation is the same as the above idealized deepwater wind generation situation, except that the water depth d is limited and constant. The computations can be compared with the expressions of the *Coastal Engineering Research Center (CERC)* [1973] and *Young and Verhagen* [1996a] and the envelope of observations reviewed by *Holthuijsen* [1980]; see Figure 10, where the dimensionless parameters are $\bar{E} = g^2 E_{tot} / U_{10}^4$, $\bar{f}_p = f_p U_{10} / g$ and $\bar{d} = gd / U_{10}^2$. The expression for the peak frequency of *CERC* [1973] is obtained here by assuming that the peak period is equal to the significant period as used in the *CERC* expression (this seems proper as the spectrum is rather peaked in shallow water [*Young and Verhagen*, 1996b]). The SWAN computations in these idealized conditions are carried out with the formulations of WAM cycle 3 adapted for shallow water with either (1) the JONSWAP bottom friction coefficient (*Hasselmann et al.* [1973] with $C_{bottom} = 0.067 \text{ m}^2 \text{ s}^{-3}$ as proposed by *Bouws and Komen* [1983] for wind sea conditions) or (2) the *Collins* [1972] model (with $C_f = 0.015$ as suggested by *Collins* [1972] or the *Madsen et al.* [1988] model with the bottom roughness length scale K_N in the expression for the friction factor f_w of *Jonsson* [1980]; $K_N = 0.05 \text{ m}$ as proposed by *Tolman* [1991]). The computational results are shown in Figure 10. These results are very similar for all three bottom friction models, and they

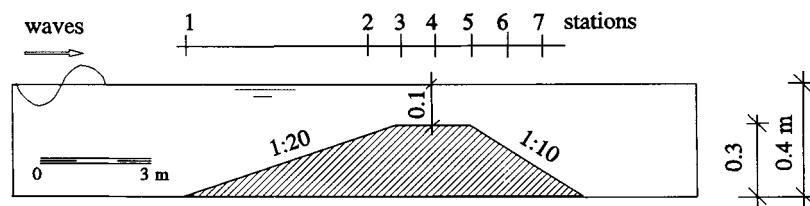


Figure 7. Experimental setup of the *Beji and Battjes* [1993] laboratory experiment with the locations of the seven wave gauges. All lengths are expressed in meters.

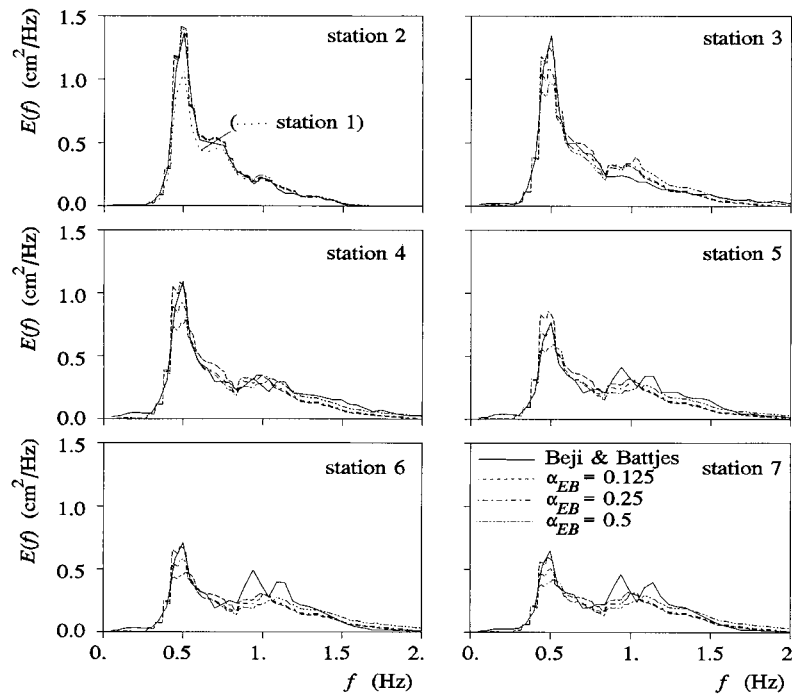


Figure 8. The spectral evolution of random waves propagating over the submerged bar at the locations of the wave gauges in the flume experiment of *Beji and Battjes* [1993]. Solid lines represent observed spectra. Dashed lines represent spectra calculated by SWAN for proportionality coefficient $\alpha_{EB} = 0.125$, $\alpha_{EB} = 0.25$, and $\alpha_{EB} = 0.5$, where EB denotes the expression of *Eldeberky* [1996].

agree reasonably well with the expressions of *CERC* [1973] and *Young and Verhagen* [1996a] and the data compiled by *Holthuijsen* [1980]. However, this test is inconclusive as to a preference for one of these three models because in very shallow water ($\bar{d} < 0.1$, say), the models of *Hasselmann et al.* [1973] and *Collins* [1972] seem to perform slightly better than the model of *Madsen et al.* [1988], whereas the reverse is true for deeper water. Additional computations are therefore carried out for fetch-limited, shallow-water situations in Lake George (near Canberra, Australia), where *Young and Verhagen* [1996a, b, c] carried out observations in nearly ideal conditions. Lake George is a fairly shallow lake with a smooth, nearly flat bottom of fine clay (no ripples, depth about 2 m; see Figure 11). It is approximately 20 km long and 10 km wide. A series of eight observation stations was situated along the north-south axis of the lake. At station 6 the wind velocity U_{10} and the directional wave spectrum were measured. From the extensive data set three typical cases were selected, i.e., with a low wind speed of $U_{10} = 6.4 \text{ m s}^{-1}$, a medium wind speed of $U_{10} = 10.8 \text{ m s}^{-1}$, and a high wind speed of $U_{10} = 15.2 \text{ m s}^{-1}$ from northerly directions (within 20° from the alignment of stations 1 through 6). Figure 12 shows the observed significant wave height H_s and peak frequency f_p at the eight stations for the three cases. Note that the observations do not always show a monotonic behavior of the waves, suggesting unresolved variations in the wind field (e.g., between stations 6 and 8 in the low-wind-speed case and at station 7 of the high-wind-speed case). *Young and Verhagen* [1996a] also found a variation in the wind speed along the north-south axis of the lake. It was systematic, and it is ascribed to the development of an atmospheric boundary layer from the upwind coast. This variation has been calculated in the present study with the expression of

Taylor and Lee [1984], as proposed by *Young and Verhagen* [1996a]. (It obviously does not resolve the anomalous wave observations.) Owing to seasonal variations and wind effects, variations in water depth were observed, which, in turn, affected considerably the location of the upwind (northern) shore. To avoid this uncertainty in the fetch, the upwave boundary for the wave model is chosen to be a straight line, through station 1, and normal to the wind direction. In the computations the incident wave condition along this upwave

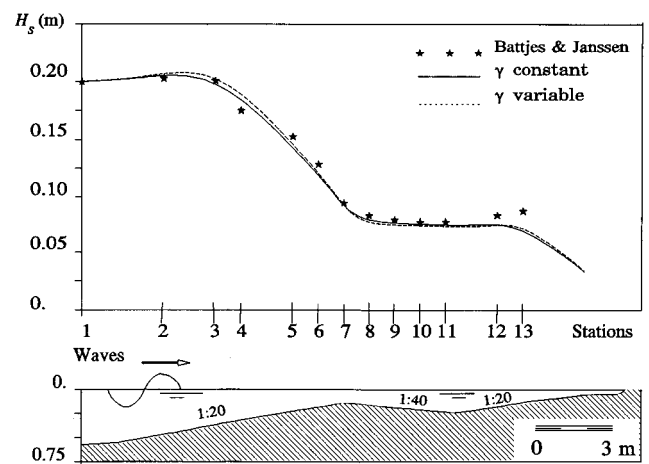


Figure 9. Depth-induced wave breaking as observed in the flume experiment of *Battjes and Janssen* [1978] and calculated with SWAN with the breaking parameter constant [*Battjes and Stive*, 1995] ($\gamma = 0.73$, solid line) and variable (modified *Nelson* [1987, 1994], $\gamma =$ analytical expression, dashed line).

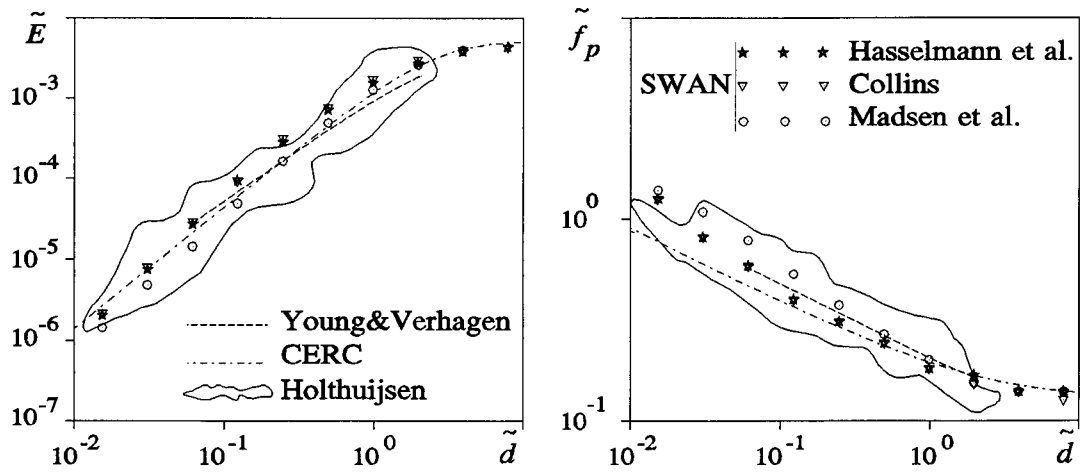


Figure 10. Shallow-water limit (infinite fetch) of (left) nondimensional total energy \tilde{E} and (right) nondimensional peak frequency \tilde{f}_p as a function of nondimensional depth \tilde{d} . Dashed lines represent the analytical expressions of Coastal Engineering Research Center (CERC) [1973] and Young and Verhagen [1996a]. Lines represent the envelope of observations reviewed by Holthuijsen [1980]. SWAN results are computed with the bottom friction formulations of Hasselmann et al. [1973] (with $C_{\text{bottom}} = 0.067 \text{ m}^2 \text{ s}^{-3}$), Collins [1972] (with bottom friction coefficient $C_f = 0.015$), and Madsen et al. [1988] (with bottom roughness length scale $K_N = 0.05 \text{ m}$).

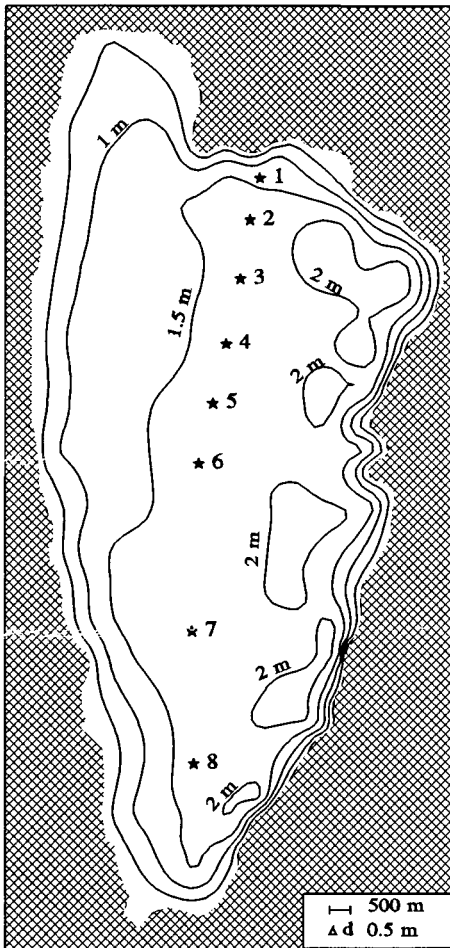


Figure 11. Bathymetry of Lake George (Australia) and locations of the eight observation stations (stars).

boundary is taken to be the observed frequency spectrum at station 1 with an assumed $\cos^2(\theta)$ directional distribution around the wind direction.

The computations have been carried out with the same values of the friction coefficients as above, except that the value of bottom roughness K_N was 0.001 m to account for the smooth character of the bottom of Lake George. The computational results for all three bottom dissipation models agree well with the observations (except at the above indicated anomalous observations). The rms error is less than 10% for both the significant wave height and the peak frequency (ignoring the anomalous observation at station 8 in the low-wind case). The JONSWAP formulation of Hasselmann et al. [1973] performed best, with an rms error of 7% (for both significant wave height and mean wave period). The results obtained with this formulation are shown in Figure 12.

As the inclusion of depth-induced breaking and triad wave-wave interactions in models for shallow-water wave growth is not conventional, the computations for the idealized shallow-water cases have been repeated with either one or the other deactivated (using the JONSWAP bottom friction formulation with $C_{\text{bottom}} = 0.067 \text{ m}^2 \text{ s}^{-3}$). It appears that the triad wave-wave interactions have practically no effect on the significant wave height or on the peak frequency (not visible on the scale of Figure 13). The effect of deactivating the depth-induced breaking is shown in Figure 13, where it is evident that only the significant wave height is slightly affected in very shallow water. The effect is generally less than that of changing the formulation of friction formulation (compare with Figure 10).

4. Discussion and Conclusions

A third-generation wave model, called Simulating Waves Nearshore (SWAN), has been developed for wave computations in coastal regions (shallow water with ambient currents).

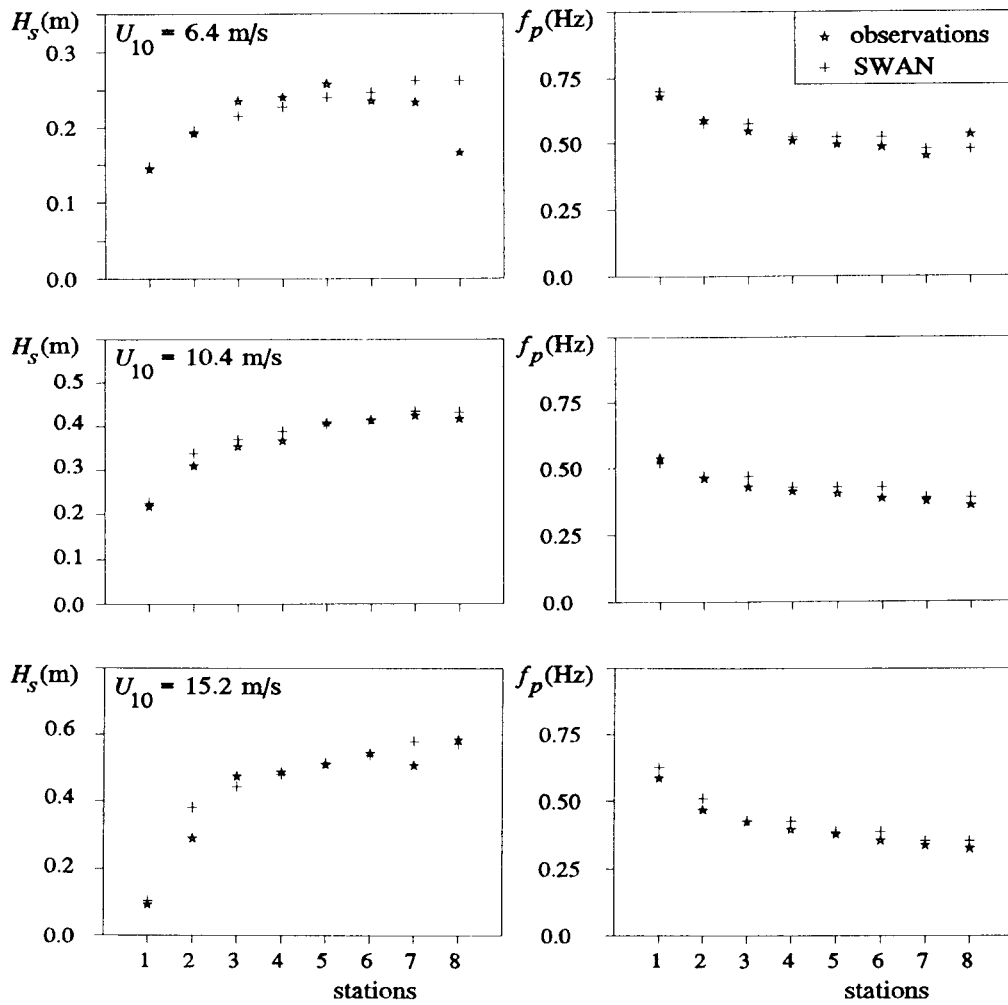


Figure 12. Observed and computed (left) significant wave height H_s and (right) peak frequency f_p in nearly ideal generation conditions at the eight stations in Lake George for three selected cases ($U_{10} = 6.4, 10.4$, and 15.2 m s^{-1} from northerly directions). SWAN results, shown at all stations, are in some cases (nearly) identical to the observations.

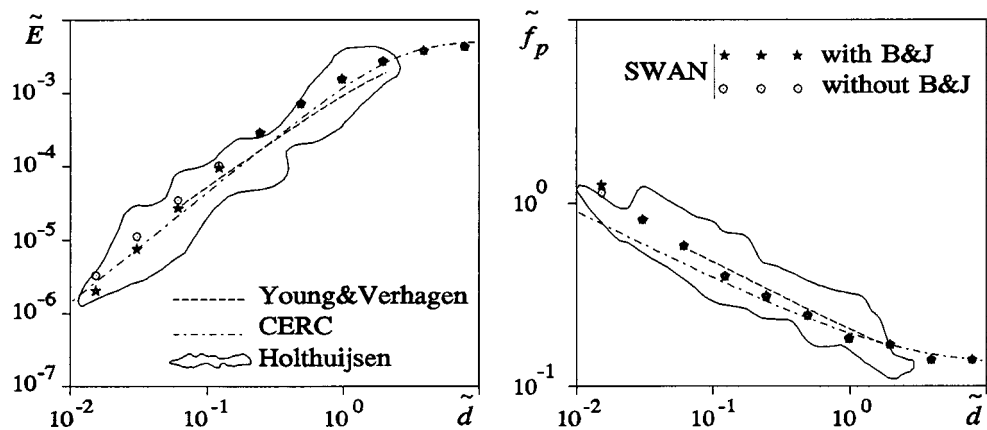


Figure 13. Same as Figure 10, but for computations with the Joint North Sea Wave Project (JONSWAP) bottom friction formulation of Hasselmann *et al.* [1973], with bottom-induced breaking (spectral version of Battjes and Janssen [1978]) activated and deactivated in the SWAN computations.

This has been achieved by (1) extending the formulations of the WAM wave model for deep water and intermediate-depth water [WAMDI Group, 1988; Komen *et al.*, 1994] by adding formulations for depth-induced wave breaking and triad wave-wave interactions and (2) by using unconditionally stable numerical techniques that are particularly suited for small-scale, shallow-water, high-resolution computations. SWAN thus accounts for the propagation of wave energy (linear wave theory for nonstationary water depths and currents), while the processes of generation and dissipation are accounted for with third-generation formulations (wind generation, whitecapping, triad and quadruplet wave-wave interactions, bottom friction, and depth-induced wave breaking). The formulation for triad wave-wave interactions and depth-induced wave breaking [Eldeberky, 1996; Eldeberky and Battjes, 1995] are new for this type of wave model. SWAN does not account for diffraction.

The numerical schemes that are used in SWAN are also new for this type of model. They are implicit rather than explicit as in other wave models such as the WAM model. The basic reason for this choice is that implicit schemes permit relatively large time steps (limited only by accuracy). This is advantageous in high-resolution situations where the time step would otherwise (for explicit schemes) be 1 or 2 orders smaller (and require correspondingly more computational effort). In stationary mode, time is removed from the model as an independent variable, allowing even more economic computations. The propagation scheme in SWAN is fairly diffusive, but since the model is intended to be used on small scales only (coastal regions with horizontal scales of less than 25 km), the effects of this are deemed to be acceptable.

Propagation tests with shoaling and refraction in deep and shallow water with and without ambient currents show excellent agreement with analytical solutions. In idealized deepwater wind generation conditions, the computational results of SWAN with the WAM cycle 3 formulations for wind input, quadruplet wave-wave interactions, and whitecapping agree very well with the expressions of Kahma and Calkoen [1992], the data compiled by Wilson [1965], and the limit values of Pierson and Moskowitz [1964]. This is not the case for the results with the WAM cycle 4 formulations [Komen *et al.*, 1994]. This is possibly due to the different choice of frequency that separates the prognostic part of the spectrum from the high-frequency diagnostic part. A test for the triad wave-wave interactions shows good agreement with the laboratory observations of Beji and Battjes [1993]. However, this test is not totally conclusive in the sense that the model results are fairly insensitive to large changes in the proportionality coefficient of the expression of triad wave-wave interactions that was used [Eldeberky, 1996]. Fortunately, the exact value of this coefficient seems to be irrelevant for the wave evolution in the cases considered in this study. A similarly good agreement is achieved in the test for depth-induced breaking where the computational results are compared with laboratory observations of Battjes and Janssen [1978]. This test indicates a slight preference for a constant ratio of maximum individual wave height over depth ($\gamma = 0.73$).

A bottom friction test, based on generalized fetch-independent, shallow-water observations (dimensionless representation) and with all of the above processes plus bottom friction active in the model, was inconclusive as to the best formulation for the bottom friction dissipation [Hasselmann *et al.*, 1973; Collins, 1972; Madsen *et al.*, 1988]. Further tests with fetch-limited, shallow-water observations in Lake George

[Young and Verhagen, 1996a] showed a slight preference for the JONSWAP formulation of Hasselmann *et al.* [1973].

SWAN seems to represent fairly well the state of the art in coastal wave modeling (within the class of linear, phase-averaged models with nonlinear sources and sinks but without diffraction). In the above academic cases the model performs well, indicating a proper numerical implementation. However, these tests are rather limited in their parameter range, and further academic testing is still necessary. More important, perhaps, are tests in real field conditions. A first series of such field tests is described in a sequel paper [Ris *et al.*, this issue].

Since SWAN is a third-generation model in which all processes of generation, propagation, and dissipation are explicitly modeled, it offers the opportunity to absorb future basic developments in the understanding of these physical processes. The model is well suited for this since it is strictly and logically modular (e.g., each source term in its own subroutine). To encourage its use for such developments and for operational purposes, SWAN has been released in the public domain (see acknowledgments).

Appendix

The complete expressions for depth-induced dissipation and the triad wave-wave interactions that are used in SWAN are given herein.

A1. Depth-Induced Wave Breaking

To model the energy dissipation in random waves due to depth-induced breaking, the bore-based model of Battjes and Janssen [1978] is used. The mean rate of energy dissipation per unit horizontal area due to wave breaking $S_{ds,br,tot}$ is expressed as

$$S_{ds,br,tot} = -\frac{1}{4} \alpha_{BJ} Q_b \left(\frac{\bar{\sigma}}{2\pi} \right) H_m^2, \quad (A1)$$

in which $\alpha_{BJ} = 1$ in SWAN and Q_b is the fraction of breaking waves determined by

$$\frac{1 - Q_b}{\ln Q_b} = -8 \frac{E_{tot}}{H_m^2}, \quad (A2)$$

in which H_m is the maximum wave height that can exist at the given depth and $\bar{\sigma}$ is a mean frequency defined as

$$\bar{\sigma} = E_{tot}^{-1} \int_0^{2\pi} \int_0^\infty \sigma E(\sigma, \theta) d\sigma c\theta. \quad (A3)$$

Extending the expression of Eldeberky and Battjes [1995] to include the spectral directions, the dissipation for a spectral component per unit time is calculated with

$$S_{ds,br}(\sigma, \theta) = -\frac{S_{ds,br,tot}}{E_{tot}} E(\sigma, \theta) \quad (A4)$$

The maximum wave height H_m is determined with $H_m = \gamma d$, in which γ is the breaker parameter (the steepness dependency in the Battjes and Janssen [1978] model is ignored here, as this steepness effect is assumed to be represented by the whitecapping process). In the literature this breaker parameter γ is often a constant or it is expressed as a function of bottom slope or incident wave steepness [see, e.g., Galvin, 1972; Battjes and Janssen, 1978; Battjes and Stive, 1985; Arcilla and Lemos,

1990; Kaminsky and Kraus, 1993; Nelson, 1987, 1994]. Since SWAN is locally defined, the dependency on incident wave steepness cannot be used. Instead, the other two options (constant value or bottom slope dependent) are used to determine the value of the breaker parameter.

Battjes and Janssen [1978], who describe the dissipation model, use a constant breaker parameter, based on Miche's criterion, of $\gamma = 0.8$. Battjes and Stive [1985] reanalyzed wave data of a number of laboratory and field experiments and found values for the breaker parameter varying between 0.6 and 0.83 for different types of bathymetry (plane, bar trough, and bar), with an average of 0.73. From a compilation of a large number of experiments, Kaminsky and Kraus [1993] found breaker parameters in the range of 0.6 to 1.59, with an average of 0.79. Nelson [1987, 1994, 1997] also (re-)analyzed laboratory and field wave data and found breaker parameters in the range of 0.55 (for horizontal bottoms) to 1.33 (for very steep slopes). He suggested the following expression for the breaker parameter for a sloping bottom (note that in the work of Nelson [1994, equation (4)] the constant 0.88 is missing in the expression of γ (R. Nelson, personal communication, 1996):

$$\gamma = H_m/d = 0.55 + 0.88 \exp[-0.012 \cot(\beta)], \quad (\text{A5})$$

in which β is the local bottom slope in the mean wave direction. This expression is based on direct observations of the ratio of the observed maximum individual wave height over local depth. However, it does not fit the data that Nelson used particularly well for $0.01 < \beta < 0.1$ [Nelson, 1987, Figure 4]. In SWAN the expression is therefore cut off (clipped) at $\beta = 0.01$ (maximum value for $\gamma = 0.81$). The bottom slope β in this expression is estimated in SWAN in the mean wave direction with a first-order upwind scheme. Since no information seems to be available for negative bottom slopes (e.g., behind sand bars), the constant value of $\gamma = 0.73$ is used for such slopes. In SWAN both the constant value of $\gamma = 0.73$ (the average value of Battjes and Stive [1985, Table 1]) and the (clipped) slope-dependent expression of Nelson [1987] are available.

A2. Triad Wave-Wave Interactions

The lumped triad approximation (LTA) of Eldeberky [1966], which is a slightly adapted version of the discrete triad approximation of Eldeberky and Battjes [1995] is used in SWAN in each spectral direction:

$$S_{nl3}(\sigma, \theta) = S_{nl3}^-(\sigma, \theta) + S_{nl3}^+(\sigma, \theta) \quad (\text{A6})$$

with

$$S_{nl3}^+(\sigma, \theta) = \max\{0, \alpha_{EB} 2\pi c c_g J^2 |\sin(\beta)| \cdot [E^2(\sigma/2, \theta) - 2E(\sigma/2, \theta)E(\sigma, \theta)]\} \quad (\text{A7})$$

$$S_{nl3}^-(\sigma, \theta) = -2S_{nl3}^+(2\sigma, \theta) \quad (\text{A8})$$

in which α_{EB} is a tunable proportionality coefficient. The bi-phase β is approximated with

$$\beta = -\frac{\pi}{2} + \frac{\pi}{2} \tanh\left(\frac{0.2}{Ur}\right) \quad (\text{A9})$$

with Ursell number Ur

$$Ur = \frac{g}{8\sqrt{2}\pi^2} \frac{H_s \bar{T}^2}{d^2} \quad (\text{A10})$$

with $\bar{T} = 2\pi/\bar{\sigma}$. The triad wave-wave interactions are ignored for $Ur < 0.1$. The interaction coefficient J is taken from Madsen and Sørensen [1993]:

$$J = \frac{k_{\sigma/2}^2 (gd + 2c_{\sigma/2}^2)}{k_{\sigma} d \left(gd + \frac{2}{15} gd^3 k_{\sigma}^2 - \frac{2}{5} \sigma^2 d^2 \right)} \quad (\text{A11})$$

Acknowledgments. We wish to acknowledge that in terms of basic concepts, we stand on the shoulders of the WAM Group, from whom we gleaned many of our ideas. This group is too large to mention all members (they are listed by Komen *et al.* [1994]), but we want to thank Gerbrand Komen of the Royal Netherlands Meteorological Institute and Klaus Hasselmann of the Max-Planck-Institut für Meteorology, Hamburg, for their inspirational role. We also want to thank Klaus and Suzanne Hasselmann for their permission to use the code of the discrete interaction approximation of the quadruplet wave-wave interactions. It was somewhat modified by Hendrik Tolman of the National Oceanic and Atmospheric Administration (United States), who shared these modifications with us. We thank him for this and also for the many discussions that we have had with him on the intricacies of numerical wave modeling. We were very fortunate to have access to the original data of the Lake George experiment of Ian Young and Louis Verhagen, University of New South Wales, Canberra, Australia, whom we hereby thank for their generosity. Jurjen Battjes of the Delft University of Technology gave us the benefit of his enthusiastic support and his well-founded suggestions in the course of this study. We thank him for this. We also thank him and Yasser Eldeberky for sharing their findings on triad wave-wave interactions in the early stages of their work on this subject. We are grateful to Cees Vuk of Delft University of Technology, whose source code of the ILU-CGSTAB solver is used in SWAN. With the sponsorship of the Office of Naval Research (United States), under grant N00014-97-1-0113 (PR number 97PR02231-00), and the Ministry of Transport, Public Works and Water Management (Netherlands), SWAN has been released in the public domain (<http://swan.ct.tudelft.nl>).

References

- Abbott, M. B., and D. R. Basco, *Computational Fluid Dynamics*, 425 pp., John Wiley, New York, 1989.
- Abreu, M., A. Larraza, and E. Thornton, Nonlinear transformation of directional wave spectra in shallow water, *J. Geophys. Res.*, 97, 15,579–15,589, 1992.
- Arcilla, A. S., and C. M. Lemos, *Surf-Zone Hydrodynamics*, 310 pp., Cent. Int. de Métodos Numer. en Ing., Barcelona, Spain, 1990.
- Arcilla, A. S., J. A. Roelvink, B. A. O'Connor, A. J. H. M. Reniers, and J. A. Jimenez, The Delta flume '93 experiment, paper presented at Coastal Dynamics Conference '94, Am. Soc. of Civ. Eng., Barcelona, Spain, 1994.
- Banner, M. L., and I. R. Young, Modelling spectral dissipation in the evolution of wind waves, I, Assessment of existing model performance, *J. Phys. Oceanogr.*, 24, 1550–1571, 1994.
- Battjes, J. A., and S. Beji, Breaking waves propagating over a shoal, in *Proceedings of 23rd International Conference on Coastal Engineering*, pp. 42–50, Am. Soc. of Civ. Eng., New York, 1992.
- Battjes, J. A., and J. P. F. M. Janssen, Energy loss and set-up due to breaking of random waves, in *Proceedings of 16th International Conference on Coastal Engineering*, pp. 569–587, Am. Soc. of Civ. Eng., New York, 1978.
- Battjes, J. A., and M. J. F. Stive, Calibration and verification of a dissipation model for random breaking waves, *J. Geophys. Res.*, 90(C5), 9159–9167, 1985.
- Battjes, J. A., M. Isaacson, and M. Quick (Eds.), Shallow water wave modelling, in *Proceedings of Waves-Physical and Numerical Modelling*, pp. 1–24, Univ. of B. C., Vancouver, 1994.
- Beji, S., and J. A. Battjes, Experimental investigation of wave propagation over a bar, *Coastal Eng.*, 19, 151–162, 1993.
- Benoit, M., F. Marcos, and F. Becq, Development of a third-generation shallow-water wave model with unstructured spatial meshing, in *Proceedings of 25th International Conference on Coastal Engineering*, pp. 465–478, Am. Soc. of Civ. Eng., New York, 1996.
- Berkhoff, J. C. W., Computation of combined refraction-diffraction, in

- Proceedings of 13th International Conference on Coastal Engineering*, pp. 471–490, Am. Soc. of Civ. Eng., New York, 1972.
- Bertotti, L., and L. Cavaleri, Accuracy of wind and wave evaluation in coastal regions, in *Proceedings of 24th International Conference on Coastal Engineering*, pp. 57–67, Am. Soc. of Civ. Eng., New York, 1994.
- Booij, N., L. H. Holthuijsen, and P. H. M. de Lange, The penetration of short-crested waves through a gap, in *Proceedings of 23rd International Conference on Coastal Engineering*, pp. 1044–1052, Am. Soc. of Civ. Eng., New York, 1992.
- Bouws, E., and G. J. Komen, On the balance between growth and dissipation in an extreme, depth-limited wind-sea in the southern North Sea, *J. Phys. Oceanogr.*, **13**, 1653–1658, 1983.
- Cardone, V. J., W. J. Pierson, and E. G. Ward, Hindcasting the directional spectra of hurricane-generated waves, *J. Pet. Technol.*, **28**, 385–394, 1976.
- Cavaleri, L., and P. Malanotte-Rizzoli, Wind wave prediction in shallow water: Theory and applications, *J. Geophys. Res.*, **86**(C11), 10,961–10,973, 1981.
- Chen, Y., R. T. Guza, and S. Elgar, Modelling of breaking surface waves in shallow water, *J. Geophys. Res.*, **102**(C11), 25,035–25,046, 1997.
- Coastal Engineering Research Center (CERC), Shore Protection Manual, *Tech. Rep. 4*, vol. I, U.S. Army Corps of Eng., Fort Belvoir, Va., 1973.
- Collins, J. I., Prediction of shallow water spectra, *J. Geophys. Res.*, **77**(15), 2693–2707, 1972.
- Dingemans, M. W., *Water Wave Propagation Over Uneven Bottoms*, part 1, *Linear Wave Propagation*, *Adv. Ser. Ocean Eng.*, vol. 13, 471 pp., World Sci., River Edge, N. J., 1997.
- Eldeberky, Y., Nonlinear transformation of wave spectra in the near-shore zone, Ph.D. thesis, Dep. of Eng., Delft Univ. of Technol., Delft, Netherlands, 1996.
- Eldeberky, Y., and J. A. Battjes, Parameterization of triad interactions in wave energy models, paper presented at Coastal Dynamics Conference '95, Am. Soc. of Civ. Eng., Gdansk, Poland, 1995.
- Eldeberky, Y., and J. A. Battjes, Spectral modelling of wave breaking: Application to Boussinesq equations, *J. Geophys. Res.*, **101**(C1), 1253–1264, 1996.
- Elgar, S., R. T. Guza, B. Raubenheimer, T. H. C. Herbers, and E. L. Gallagher, Spectral evolution of shoaling and breaking waves on a barred beach, *J. Geophys. Res.*, **102**(C7), 15,797–15,805, 1997.
- Ewing, J. A., A numerical wave prediction method for the North Atlantic Ocean, *Dtsch. Hydrogr. Z.*, **24**(6), 241–261, 1971.
- Freilich, M. H., and R. T. Guza, Nonlinear effects on shoaling surface gravity waves, *Philos. Trans. R. Soc. London, Ser. A*, **A311**, 1–41, 1984.
- Galvin, C. J., *Wave Breaking in Shallow Water, Waves on Beaches and Resulting Sediment Transport*, pp. 413–455, Academic, San Diego, Calif., 1972.
- Gelci, R., H. Cazalé, and J. Vassal, Utilization des diagrammes de propagation à la prévision énergétique de la houle (in French), *Info. Bull.* **8**(4), pp. 160–197, Com. Cent. d'Océanogr. et d'Études des Côtes, Paris, 1956.
- Golub, G. H., and C. F. van Loan, *Matrix Computations*, 476 pp., Academic, San Diego, Calif., 1986.
- Günther, H., S. Hasselmann, and P. A. E. M. Janssen, The WAM model cycle 4 (revised version), *Tech. Rep. 4*, Deutsch. Klimatol. Rechenzentrum, Hamburg, Germany, 1992.
- Hasselmann, K., On the spectral dissipation of ocean waves due to whitecapping, *Bound.-layer Meteor.*, **6**, 1–2, 107–127, 1974.
- Hasselmann, K., and J. I. Collins, Spectral dissipation of finite-depth gravity waves due to turbulent bottom friction, *J. Mar. Res.*, **26**, 1–12, 1968.
- Hasselmann, S., and K. Hasselmann, A symmetrical method of computing the non-linear transfer in a gravity-wave spectrum, *Geophys. Einzelschr.*, *Ser. A*, **52**(8), Geophys. Inst., Univ. of Hamburg, Hamburg, Germany, 1981.
- Hasselmann, K., et al., Measurements of wind-wave growth and swell decay during the Joint North Sea Wave Project (JONSWAP), *Dtsch. Hydrogr. Z. Suppl.*, **12**(A8), 1–95, 1973.
- Hasselmann, K., D. B. Ross, P. Müller, and W. Sell, A parametric wave prediction model, *J. Phys. Oceanogr.*, **6**, 200–228, 1976.
- Hasselmann, S., K. Hasselmann, J. H. Allender, and T. P. Barnett, Computations and parameterizations of the linear energy transfer in a gravity wave spectrum, II, Parameterizations of the nonlinear transfer for application in wave models, *J. Phys. Oceanogr.*, **15**, 1378–1391, 1985.
- Hedges, T. S., Combination of waves and currents: An introduction, *Proc. Inst. Civ. Eng., Part 1*, **82**, 567–585, 1987.
- Holthuijsen, L. H., Methods of wave prediction, I and II (in Dutch), report Tech. Adv. Comm. Against Inundation, Den Haag, Netherlands, 1980.
- Holthuijsen, L. H., and S. De Boer, Wave forecasting for moving and stationary targets, in *Computer Modelling in Ocean Engineering*, edited by B. Y. Schrefler and O. C. Zienkiewicz, pp. 231–234, A. A. Balkema, Rotterdam, Netherlands, 1988.
- Holthuijsen, L. H., N. Booij, and T. H. C. Herbers, A prediction model for stationary, short-crested waves in shallow water with ambient currents, *Coastal Eng.*, **13**, 23–54, 1989.
- Janssen, P. A. E. M., Quasi-linear theory of wind-wave generation applied to wave forecasting, *J. Phys. Oceanogr.*, **21**, 1631–1642, 1991a.
- Janssen, P. A. E. M., Consequences of the effect of surface gravity waves on the mean air flow, paper presented at Breaking Waves, Int. Union of Theor. and Appl. Mech., Sydney, Australia, 1991b.
- Jonsson, I. G., Wave boundary layers and friction factors, in *Proceedings of 10th International Conference on Coastal Engineering*, pp. 127–148, Am. Soc. of Civ. Eng., New York, 1966.
- Jonsson, I. G., A new approach to rough turbulent boundary layers, *Ocean Eng.*, **7**, 109–152, 1980.
- Jonsson, I. G., Wave current interactions, in *The Sea, Ocean Eng. Sci. Ser.*, vol. 9, part A, edited by B. Le Mehaute and D. M. Hanes, pp. 65–70, John Wiley, New York, 1993.
- Jonsson, I. G., and N. A. Carlsen, Experimental and theoretical investigations in an oscillatory turbulent boundary layer, *J. Hydraul. Res.*, **14**, 45–60, 1976.
- Kahma, K. K., and C. J. Calkoen, Reconciling discrepancies in the observed growth of wind-generated waves, *J. Phys. Oceanogr.*, **22**, 1389–1405, 1992.
- Kaminsky, G. M., and N. C. Kraus, Evaluation of depth-limited wave breaking criteria, paper presented at 2nd International Symposium on Ocean Wave Measurement and Analysis, Waterw., Port, Coastal and Ocean Div., Am. Soc. of Civ. Eng., New Orleans, La., 1993.
- Kirby, J. T., Higher-order approximation in the parabolic equation method for water waves, *J. Geophys. Res.*, **91**(C1), 933–952, 1986.
- Komen, G. J., S. Hasselmann, and K. Hasselmann, On the existence of a fully developed wind-sea spectrum, *J. Phys. Oceanogr.*, **14**, 1271–1285, 1984.
- Komen, G. J., L. Cavaleri, M. Donelan, K. Hasselmann, S. Hasselmann, and P. A. E. M. Janssen, *Dynamics and Modelling of Ocean Waves*, 532 pp., Cambridge Univ. Press, New York, 1994.
- Kuik, A. J., G. P. van Vledder, and L. H. Holthuijsen, A method for the routine analysis of pitch-and-roll buoy wave data, *J. Phys. Oceanogr.*, **18**, 1020–1034, 1988.
- Li, C. W., and M. Mao, Spectral modelling of typhoon-generated waves in shallow waters, *J. Hydraul. Res.*, **30**, 611–622, 1992.
- Luo, W., and J. Monbaliu, Effects of the bottom friction formulation on the energy balance for gravity waves in shallow water, *J. Geophys. Res.*, **99**(C9), 18,501–18,511, 1994.
- Madsen, O. S., Y.-K. Poon, and H. C. Graber, Spectral wave attenuation by bottom friction: Theory, in *Proceedings of 21th International Conference on Coastal Engineering*, pp. 492–504, Am. Soc. of Civ. Eng., New York, 1988.
- Madsen, P. A., and O. R. Sørensen, A new form of the Boussinesq equations with improved linear dispersion characteristics, 2, A slowly-varying bathymetry, *Coastal Eng.*, **18**, 183–205, 1992.
- Madsen, P. A., and O. R. Sørensen, Bound waves and triad interactions in shallow water, *Ocean Eng.*, **20**, 359–388, 1993.
- Mase, H., and J. T. Kirby, Hybrid frequency-domain KdV equation for random wave transformation, in *Proceedings of 23rd International Conference on Coastal Engineering*, pp. 474–487, Am. Soc. of Civ. Eng., New York, 1992.
- Mastenbroek, C., G. Burgers, and P. A. E. M. Janssen, The dynamical coupling of a wave model in a storm surge model through the atmospheric boundary layer, *J. Phys. Oceanogr.*, **23**, 1856–1866, 1993.
- Miles, J. W., On the generation of surface waves by shear flows, *J. Fluid Mech.*, **3**, 185–204, 1957.
- Miles, J. W., Hamiltonian formulations for surface waves, *Appl. Sci. Res.*, **37**, 103–110, 1981.
- Nelson, R. C., Design wave heights on very mild slopes: An experi-

- mental study, *Civil. Eng. Trans.* 29, pp. 157–161, Inst. of Eng. Aust., Barton, 1987.
- Nelson, R. C., Depth limited wave heights in very flat regions, *Coastal Eng.*, 23, 43–59, 1994.
- Nelson, R. C., Height limits in top down and bottom up wave environments, *Coastal Eng.*, 32, 247–254, 1997.
- Peregrine, D. H., Long waves on a beach, *J. Fluid Mech.*, 27, 815–827, 1966.
- Phillips, O. M., On the generation of waves by turbulent wind, *J. Fluid Mech.*, 2, 417–445, 1957.
- Phillips, O. M., *The Dynamics of the Upper Ocean*, 336 pp., Cambridge Univ. Press, New York, 1977.
- Phillips, O. M., Spectral and statistical properties of the equilibrium range in wind-generated gravity waves, *J. Fluid Mech.*, 156, 505–531, 1985.
- Pierson, W. J., and L. Moskowitz, A proposed spectral form for fully developed wind seas based on the similarity theory of S. A. Kitaigorodskii, *J. Geophys. Res.*, 69(24), 5181–5190, 1964.
- Piest, J., Seegangsbestimmung und Seegangsrefraktion in einem Meer mit nichtebenem Boden; eine theoretische Untersuchung (in German), *Dtsch. Hydrogr. Z.*, 18, 67–74, 1965.
- Radder, A. C., On the parabolic equation method for water-wave propagation, *J. Fluid Mech.*, 95, 159–176, 1979.
- Radder, A. C., An explicit Hamiltonian formulation of surface waves in water of finite depth, *J. Fluid Mech.*, 237, 435–455, 1992.
- Resio, D., and W. Perrie, A numerical study of nonlinear energy fluxes due to wave-wave interactions, I, Methodology and basic results, *J. Fluid Mech.*, 223, 609–629, 1991.
- Ris, R. C., L. H. Holthuijsen, and N. Booij, A third-generation wave model for coastal regions, 2, Verification, *J. Geophys. Res.*, this issue.
- Roache, P. J., *Computational Fluid Dynamics*, 446 pp., Hermosa, Albuquerque, N. M., 1972.
- Shemdin, P., K. Hasselmann, S. V. Hsiao, and K. Herterich, Non-linear and linear bottom interaction effects in shallow water, in *Turbulent Fluxes Through the Sea Surface, Wave Dynamics and Prediction*, NATO Conf. Ser., vol. V(1), 347–372, 1978.
- Snyder, R. L., F. W. Dobson, J. A. Elliott, and R. B. Long, Array measurement of atmospheric pressure fluctuations above surface gravity waves, *J. Fluid Mech.*, 102, 1–59, 1981.
- SWAMP Group, *Ocean Wave Modelling*, 256 pp., Plenum, New York, 1985.
- Taylor, P. A., and R. J. Lee, Simple guidelines for estimating wind speed variations due to small-scale topographic features, *Climatol. Bull.*, 18, 3–32, 1984.
- Thornton, E. B., and R. T. Guza, Transformation of wave height distribution, *J. Geophys. Res.*, 88(C10), 5925–5938, 1983.
- Tolman, H. L., A third-generation model for wind waves on slowly varying, unsteady and inhomogeneous depths and currents, *J. Phys. Oceanogr.*, 21, 782–797, 1991.
- Tolman, H. L., Effects of numerics on the physics in a third-generation wind-wave model, *J. Phys. Oceanogr.*, 22, 1095–1111, 1992a.
- Tolman, H. L., An evaluation of expressions for the wave energy dissipation due to bottom friction in the presence of currents, *Coastal Eng.*, 16, 165–179, 1992b.
- Van der Vorst, H. A., Bi-CGSTAB: A fast and smoothly converging variant of Bi-CG for solution of non-symmetric linear systems, *SIAM J. Sci. Stat. Comput.*, 13, 631–644, 1992.
- Van Vledder, G. P., J. G. de Ronde, and M. J. F. Stive, Performance of a spectral wind-wave model in shallow water, in *Proceedings of 24th International Conference on Coastal Engineering*, pp. 761–774, Am. Soc. of Civ. Eng., New York, 1994.
- Vincent, C. L., J. M. Smith, and J. Davis, Parameterization of wave breaking in models, in *Proceedings of International Symposium: Waves—Physical and Numerical Modelling*, vol. 2, edited by M. Isaacson and M. Quick, pp. 753–762, Univ. of B. C., Vancouver, 1994.
- Vuik, C., Solution of the discretized incompressible Navier-Stokes equations with the GMRES method, *Int. J. Numer. Methods Fluids*, 16, 507–523, 1993.
- WAMDI Group, The WAM model—A third generation ocean wave prediction model, *J. Phys. Oceanogr.*, 18, 1775–1810, 1988.
- Weber, S. L., Surface gravity waves and turbulent bottom friction, Ph.D. thesis, Univ. of Utrecht, Utrecht, Netherlands, 1989.
- Weber, S. L., Bottom friction for wind sea and swell in extreme depth-limited situations, *J. Phys. Oceanogr.*, 21, 149–172, 1991a.
- Weber, S. L., Eddy-viscosity and drag-law models for random ocean wave dissipation, *J. Fluid Mech.*, 232, 73–98, 1991b.
- Whitham, G. B., *Linear and Nonlinear Waves*, 636 pp., John Wiley, New York, 1974.
- Wilson, B. W., Numerical prediction of ocean waves in the North Atlantic for December 1959, *Dtsch. Hydrogr. Z.*, 18, 114–130, 1965.
- Wu, J., Wind-stress coefficients over sea surface from breeze to hurricane, *J. Geophys. Res.*, 87(C12), 9704–9706, 1982.
- Yamaguchi, M., A numerical model for refraction computation of irregular waves due to time-varying currents and water depth, in *Proceedings of 22nd International Conference on Coastal Engineering*, pp. 205–217, Am. Soc. of Civ. Eng., 1990.
- Yan, L., An improved wind input source term for third generation ocean wave modelling, *Sci. Rep. WR 87-8*, R. Neth. Meteorol. Inst., De Bilt, 1987.
- Young, I. R., A shallow water spectral wave model, *J. Geophys. Res.*, 93(C5), 5113–5129, 1988.
- Young, I. R., and M. L. Banner, Numerical experiments on the evolution of fetch limited waves, paper presented at Int. Union of Theor. and Appl. Mech. (IUTAM), Sydney, Australia, 1992.
- Young, I. R., and G. P. van Vledder, A review of the central role of nonlinear interactions in wind-wave evolution, *Philos. Trans. R. Soc. London, Ser. A*, 342, 505–524, 1993.
- Young, I. R., and L. A. Verhagen, The growth of fetch limited waves in water of finite depth, 1, Total energy and peak frequency, *Coastal Eng.*, 29, 47–78, 1996a.
- Young, I. R., and L. A. Verhagen, The growth of fetch limited waves in water of finite depth, 2, Spectral evolution, *Coastal Eng.*, 29, 79–99, 1996b.
- Young, I. R., and L. A. Verhagen, The growth of fetch limited waves in water of finite depth, 3, Directional spectra, *Coastal Eng.*, 29, 101–121, 1996c.

N. Booij and L. H. Holthuijsen (corresponding author), Faculty of Civil Engineering, Delft University of Technology, Stevinweg 1, 2628 CN, Delft, Netherlands. (N.Booij@ct.tudelft.nl; L. Holthuijsen@ct.tudelft.nl)
 R. C. Ris, WL/Delft Hydraulics, Rotterdamseweg 185, 2629 HD, Delft, Netherlands. (Roeland.Ris@wldelft.nl)

(Received June 16, 1997; revised March 3, 1998; accepted May 29, 1998.)